UNIVERSITÀ DEGLI STUDI DI PADOVA
Department of Comparative Biomedicine and Food Science

Second Cycle Degree (MSc) in
Biotechnologies for Food Science

# Triplex-Mediated Polyamines Effect on Gene Expression

Supervisor
Prof. Fabio Vianello

Co-supervisor
Dr. Alessandro Cecconello

Submitted by
Yeganeh Daeizadehjeloudar

Student n. 2087202

ACADEMIC YEAR 2024-2025

UNIVERSITÀ DEGLI STUDI DI PADOVA
Dipartimento di Biomedicina Comparata e Alimentazione

Corso di Laurea Magistrale in
Biotechnologies for Food Science

# Effetti regolatori di poliammine e triplex sull'espressione genetica

Relatore
Prof. Fabio Vianello

Correlatore
Dott. Alessandro Cecconello

Laureanda
Yeganeh Daeizadehjeloudar

Matricola n. 2087202

ANNO ACCADEMICO 2024-2025

# Acknowledgements

This work would not have been possible without the guidance, patience, and support of those who stood by every step of the way. My deepest gratitude goes to Professor Vianello and Dr. Cecconello, whose encouragement and insightful advice shaped this thesis. Their patience, constructive feedback, and open-minded approach made even the most challenging moments more manageable. Their support and belief in this work provided the confidence to push forward, even when progress felt uncertain.

A special thanks to Aura, who was always there when things felt overwhelming. In moments of doubt and exhaustion, she reminded me that giving up was never an option. Her generosity in sharing her knowledge and her constant encouragement made this journey far less daunting.

To the friends who stood by through every challenge—whether through long conversations, shared frustrations, or quiet reassurance—their presence, even from afar, made all the difference. Their support, in both big and small ways, meant more than words can express.

And finally, to the two people who have been the foundation of everything—my mom and dad. Without their love, sacrifices, and unwavering belief in me, none of this would have been possible. This achievement is not mine alone; it belongs to them just as much as it does to the one who wrote these words.

## Dedication

To the women whose work was erased, whose voices were silenced, whose dreams were dismissed before they had the chance to grow, and to every one of them who unsettled inherited conformity.

# Abstract

In this experimental thesis work, triple-helix complexes composed of an RNA strand and a DNA double helix were investigated, along with their effect on transcription. These complexes, known as triplexes, were first predicted in the 1950s and later synthesized in vitro in more recent years, as reported in scientific literature. Although their experimental validation in living cells remains an active area of research, several studies now support their existence and dual functionality: (i) as genomic structural elements influencing chromatin architecture, and (ii) as regulatory elements modulating gene expression.

This thesis focused on the biophysical mechanisms by which triplexes are stabilized in physiological environments by biomolecules containing amine groups, with a particular emphasis on the polyamines spermine, spermidine, cadaverine, and putrescine. This aspect is central to the study of triplexes because their charge density per nucleotide pair is higher than that of a DNA duplex, necessitating a mechanism to mitigate electrostatic repulsion.

Electrophoretic mobility shift assays (EMSA) and temperature-dependent dissociation analyses (melting temperature, Tm, analysis) were conducted to estimate thermodynamic parameters, such as the dissociation constant, enabling the comparison of triplex stability under different conditions. The results demonstrated that among the polyamines tested, spermine and spermidine provided the highest stabilization of the triplex, comparable to the effects of high $Mg^{2+}$ concentrations.

Further molecular modelling and mass spectrometry analyses confirmed the EMSA and Tm analysis data, revealing the geometry of the triplex-polyamine complex in a model triplex sequence of 15 nucleotides. The effect of triplex formation on transcriptional modulation represents the next step in this research, with preliminary results presented in this work. The findings of this thesis are currently part of a scientific article in preparation for publication.

# Sommario

In questo lavoro di tesi sperimentale, sono stati investigati complessi a tripla elica composti da un filamento di RNA e una doppia elica di DNA e il loro effetto sulla trascrizione. Questi complessi sono chiamati triplex e sono noti in letteratura scientifica per essere stati predetti negli anni ’50 e successivamente prodotti in vitro in anni recenti. Nonostante la loro verifica sperimentale in cellula sia ancora oggetto di ricerca, ci sono ormai diversi studi che indicano la loro esistenza e la loro duplice funzione: (i) elementi strutturali genomici che influenzano l’architettura della cromatina e (ii) elementi regolatori che regolano l’espressione dei geni. Questa tesi si è occupata di studiare da un punto di vista biofisico come i triplex siano stabilizzati in ambiente fisiologico da parte di biomolecole contenenti gruppi amminici e in particolare concentrandosi sulle poliammine spermina, spermidina, cadaverina e putrescina. Questo aspetto è centrale nello studio dei triplex perché la densità di carica elettrica nel complesso triplex è più elevata di un duplex di DNA, per coppia di nucleotidi, e richiede un meccanismo di riduzione della repulsione elettrostatica. Esperimenti di elettroforesi (electrophoretic mobility shift assay, EMSA) e dissociazione temperatura-dipendente (melting temperature, Tm, analysis) condotti in questo lavoro, hanno portato alla stima di parametri termodinamici come la costante di dissociazione che ha permesso il confronto della stabilità dei triplex in diverse condizioni. I risultati hanno dimostrato che, tra le poliammine, spermina e spermidina stabilizzano maggiormente il triplex, a livelli comparabili ad elevate concentrazioni di $Mg^{2+}$. Ulteriori dati di modellizzazione molecolare e analisi di massa, hanno confermano i dati EMSA e Tm analysis, rivelando la geometria del complesso triplex-poliammine in un triplex modello lungo 15 nucleotidi. L’effetto di modulazione della trascrizione è il passo successivo di questo del quale vengono presentati dei risultati preliminari. I risultati di questa tesi sono attualmente parte di un articolo scientifico di prossima pubblicazione.

# TABLE OF CONTENTS

# 1. INTRODUCTION

## 1.1. Nucleic Acids: Functions and Structural Features

DNA (deoxyribonucleic acid) and RNA (ribonucleic acid) are key biomolecules that store, transmit, and mediate the expression of genetic information. DNA serves as the genetic repository for living organisms, encoding the instructions necessary for their development, metabolism, and reproduction. RNA, on the other hand, plays versatile roles in the cell, functioning as a carrier of genetic information, a regulatory molecule, and even as a catalyst in various biochemical reactions.[1], [2]

DNA, a nucleotide-based molecule organized in a double-helical structure, functions as the primary repository of genetic information. Its four nitrogenous bases—adenine (A), thymine (T), cytosine (C), and guanine (G)—are linked through a sugar-phosphate backbone, forming the core framework of the molecule. The sugar component, deoxyribose, is a key distinguishing feature, as it lacks a hydroxyl group at the 2' position in contrast to ribose. This structural difference reduces the vulnerability of DNA to hydrolytic cleavage, significantly enhancing its chemical stability and making it suitable for long-term genetic information storage.[3]

The primary structure of DNA leads to the formation of a double-stranded helix through canonical Watson-Crick base pairing—hydrogen bonds between adenine and thymine (two bonds), and guanine and cytosine (three bonds). These interactions ensure the stability of the double helix, making DNA suitable for maintaining genetic integrity during replication and transcription.[2]

The DNA double helix exhibits a consistent structural organization, with a diameter of approximately 2 nm and a helical repeat of 3.4 nm per turn, comprising 8–10 base pairs per helical cycle. The sugar-phosphate backbone is positioned externally, while the nitrogenous bases are oriented internally, forming hydrogen bonds that stabilize the structure. The helical conformation generates distinct major and minor grooves, which serve as critical

binding sites for DNA-associated proteins, thereby facilitating regulatory processes such as transcription and chromatin remodelling (Figure 1).

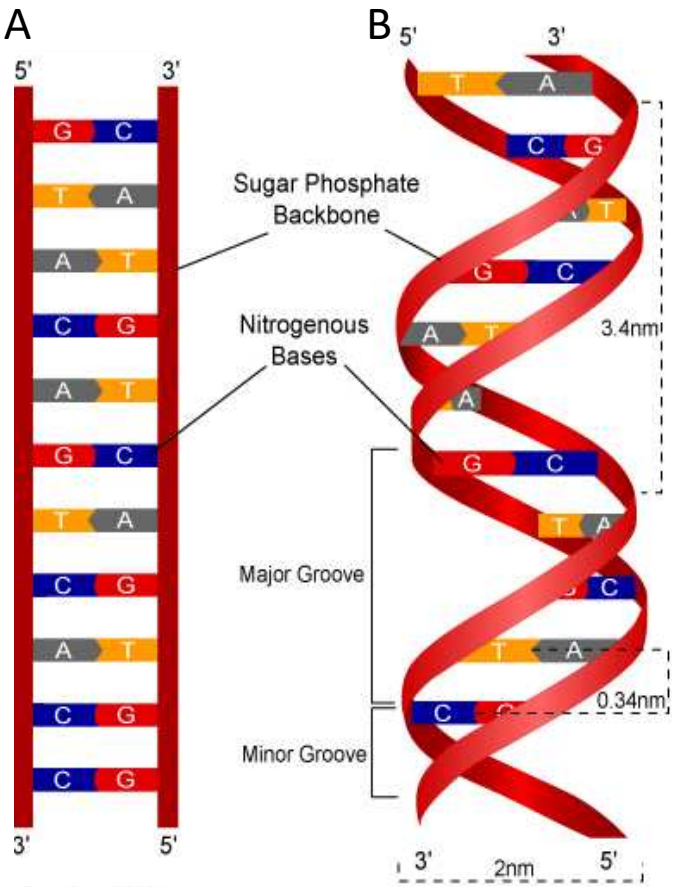


*Figure 1: (A) DNA helix illustrating helical dimensions and base pairing. (B) Molecular model showing the backbone and groove structure. Reproduced with modifications from (Dept. Biol., Penn State, 2004).*

Figure 2 shows canonical and non-canonical base pairs. While Watson-Crick base pairs represent the predominant structural form of DNA, additional secondary structures can form under specific conditions, adding layers of regulation and flexibility. These non-canonical structures arise in particular genomic contexts, such as telomeres or promoter regions, where they play roles in modulating protein binding and gene activity by either facilitating or restricting access to genetic information and serve as regulatory elements that influence the expression and stability of the genome.[4], [5]

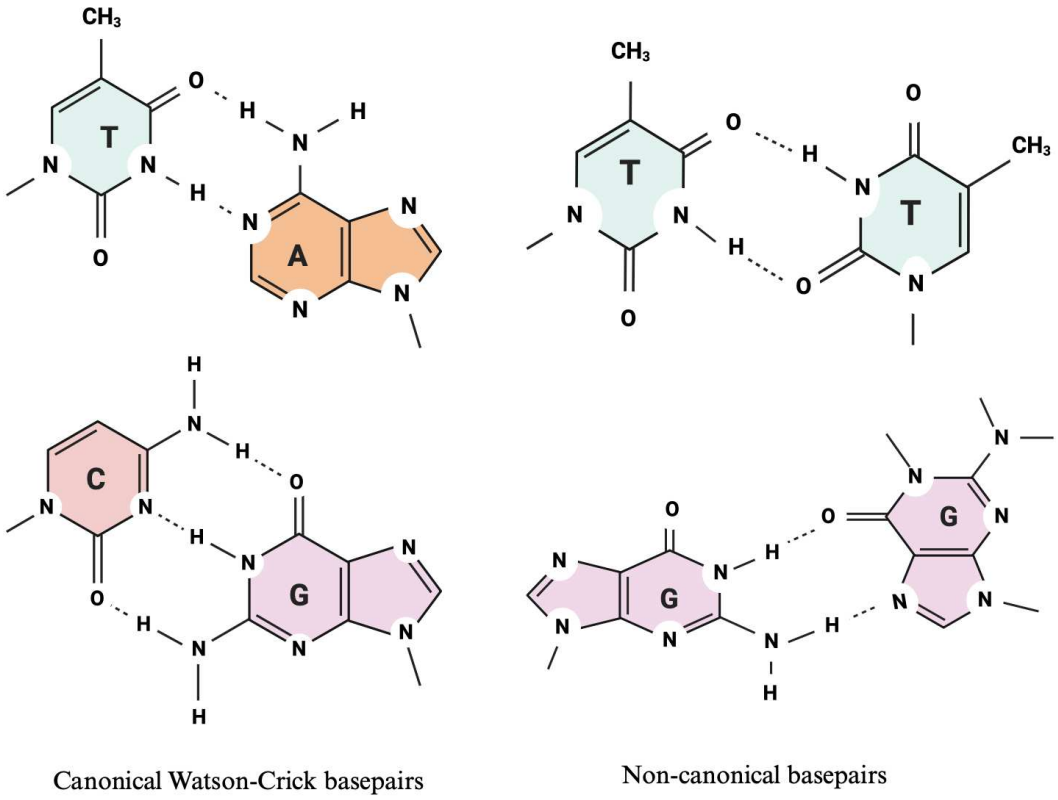


*Figure 2: Canonical and non-canonical (such as G-G and T-T) base pairs, highlighting distinct hydrogen bonding patterns. Created with BioRender*

More importantly, both canonical and non-canonical base pairings contribute to the formation of more complex configurations, including DNA-RNA hybrids, which play crucial roles in regulating gene expression.[6]

These non-canonical structures, NCS, include:

- G-quadruplexes: These are four-stranded structures formed through Hoogsteen hydrogen bonding in guanine-rich regions of the DNA. These structures are typically found in telomeres and promoter regions of genes and are stabilized by the presence of monovalent cations, such as potassium ions. The biological relevance of G-quadruplexes extends to processes such as telomere maintenance, where they prevent telomerase access, and transcriptional regulation, where they influence promoter accessibility.[5]

- i-motifs: The i-motif is a four-stranded structure found in cytosine-rich regions, forming under acidic conditions due to the protonation of cytosine bases. Unlike G-quadruplexes, i-motifs are more transient at physiological pH but are implicated in transcriptional regulation by altering the local structure of gene promoters. These structures modulate the accessibility of certain genomic regions, thereby influencing gene expression during specific cellular states, such as stress responses.[5]

- Figure 3 represents the structures of a G-quadruplex and an i-motif. Grey squares in the G-quadruplex scheme represent tetrads of guanines (G) linked by Hoogsteen hydrogen bonds. These bonds are stabilized by the metal ions ($M^+$). The i-motif structure is stabilized "intercalated" hydrogen bonds that cross the structure centre, between cytosines (C) and protonated cytosines ($C^+$).

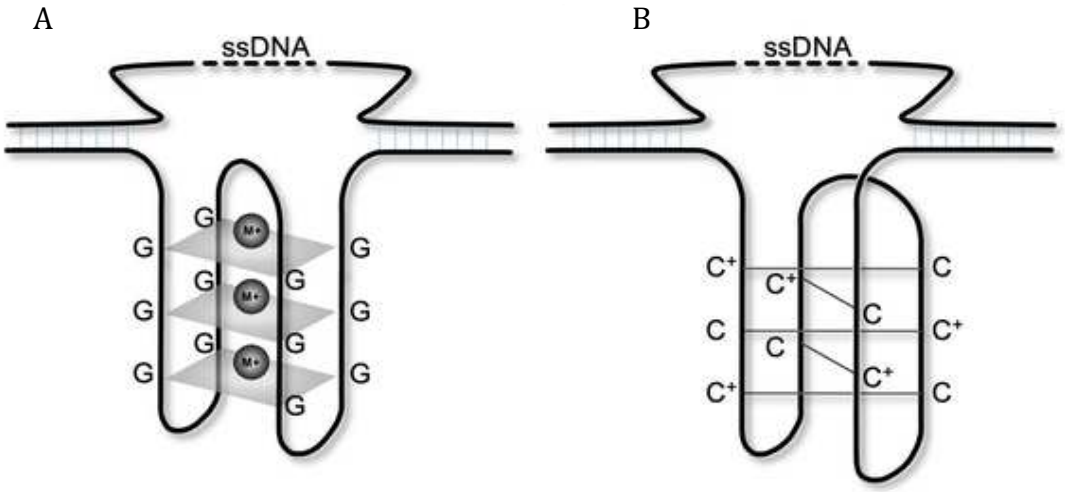


*Figure 3: G-quadruplex (A), i-motif (B) Reproduced with modifications from ref.[6]*

RNA is predominantly single-stranded, allowing it to form a variety of complex shapes that contribute to its functional versatility. The nucleotide bases in RNA are adenine (A), uracil (U), cytosine (C), and guanine (G). RNA sugar component, ribose, contains a hydroxyl group at the 2' position, which increases its chemical reactivity, making it more susceptible to hydrolysis. As a result, RNA is typically less stable than DNA, facilitating its role in transient and regulatory functions.[2], [7]

Figure 4 illustrates the hierarchical organization of RNA structure, highlighting its three structural levels. The primary structure consists of a linear nucleotide sequence, which

rapidly folds into a secondary structure through intramolecular base pairing, forming helices and loops. Further folding interactions result in the formation of a tertiary structure, where complex three-dimensional conformations emerge, enabling RNA's functional diversity.

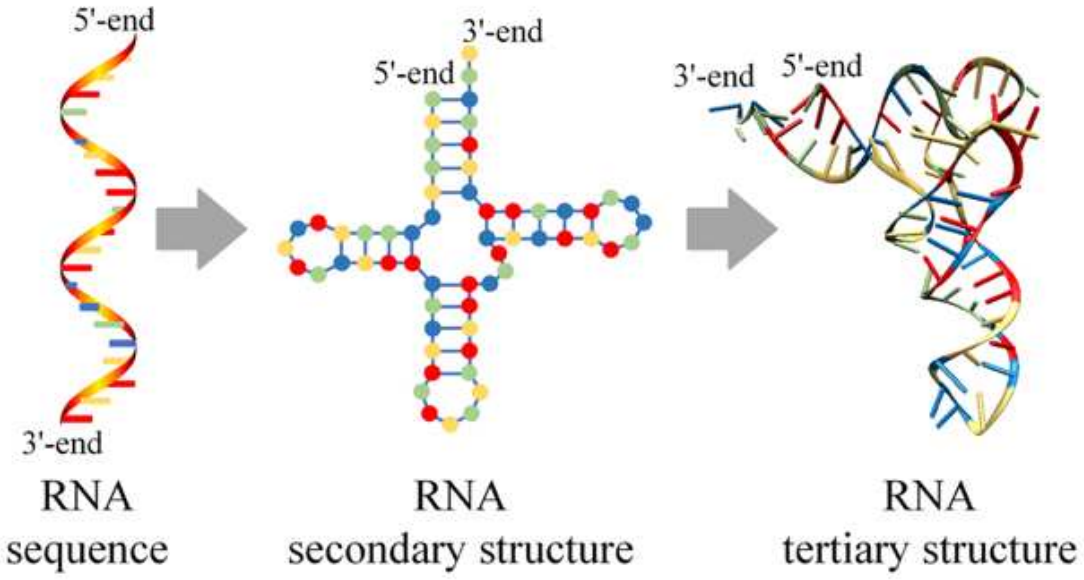


*Figure 4: RNA structural hierarchy: Primary (linear), secondary (base-paired), and tertiary (3D folded) structures. Reproduced from ref.* ***[8]***

In RNA, canonical Watson-Crick base pairing also plays an important role, with adenine pairing with uracil instead of thymine. Additionally, non-canonical interactions are critical for stabilizing RNA secondary structures and facilitating intricate tertiary interactions, which underlie many of its biological functions. Unlike the strict pairing rules of canonical Watson-Crick interactions, non-canonical base pairings offer RNA the flexibility needed to form unique secondary and tertiary structures that are essential for complex cellular functions. These pairings are crucial for RNA adaptability, allowing it to perform diverse roles such as catalysis and regulation.

Non-canonical pairings include:

- G-U Wobble Pairing: This type of pairing occurs between guanine (G) and uracil (U) through weaker hydrogen bonds compared to canonical pairs. G-U wobble pairing is one of the most common non-canonical interactions in RNA, providing the molecule with structural flexibility and the ability to form unique three-dimensional conformations.[7]

- A-A and G-A Pairs: Adenine (A) can pair with another adenine (A) or a guanine (G), forming non-canonical pairs that stabilize specific structural motifs. These pairings often appear in internal loops and contribute to the formation of complex RNA folds.

- C-U and A-C Pairs: In certain regions, cytosine (C) may pair with uracil (U) or adenine (A), which further contributes to the structural diversity of RNA, particularly in loops and bulges.[7]

RNA exhibits a wide variety of secondary structures, each with specific functional implications. These structures include:

- Stem-loops and hairpins: Stem-loops are formed when an RNA strand folds back on itself, creating a double-stranded stem region with an unpaired loop. Hairpins are shorter versions of stem-loops and are often used as recognition motifs by regulatory proteins involved in mRNA stability and translation regulation. For example, hairpin structures in tRNA facilitate recognition by the ribosome and help initiate the translation process.[7], [9]

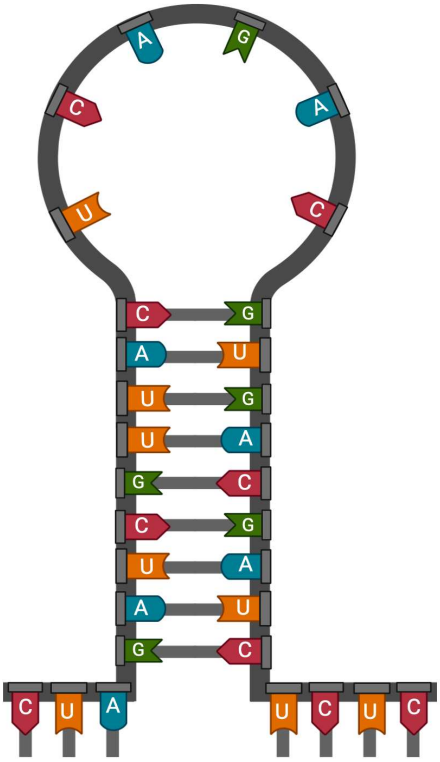


Figure 5: RNA structural motif: Hairpin. Created with BioRender

- Bulges: Bulges occur when unpaired nucleotides are present within a double-stranded RNA segment, creating an asymmetric structure. These structures often serve as binding sites for RNA-binding proteins, such as splicing factors involved in the regulation of alternative splicing. Bulges add flexibility to the RNA molecule, enabling it to interact with different protein partners in complex regulatory processes.[7]

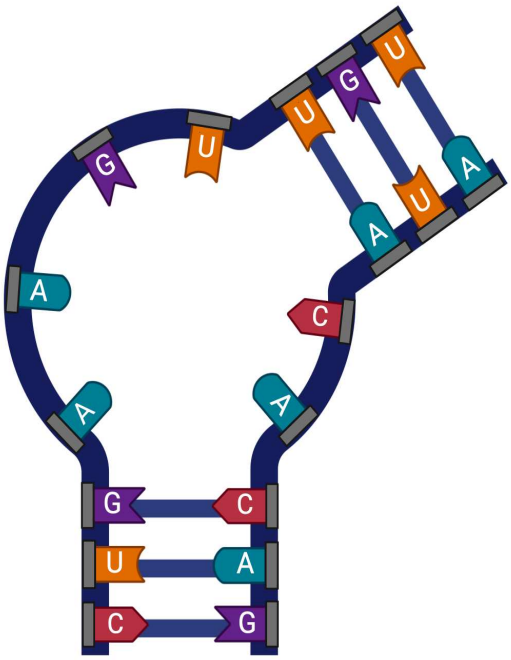


Figure 6: RNA structural motif: Bulge. Created with BioRender

- Pseudoknots: A pseudoknot forms when bases within a loop region pair with complementary bases elsewhere in the RNA molecule, creating a three-dimensional structure. Pseudoknots are integral to processes such as ribosomal frameshifting, which is commonly utilized by RNA viruses like HIV to maximize coding potential. In addition, pseudoknots stabilize ribozymes and contribute to catalytic activity by creating precise active sites required for catalysis.[7], [9]

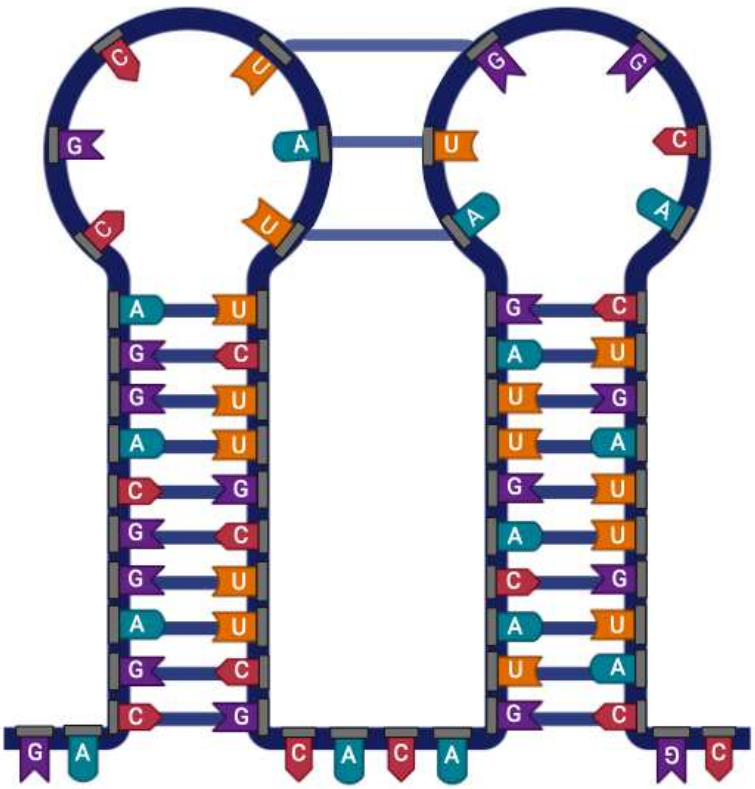

*Figure 7: RNA structural motif: Pseudoknot. Created with BioRender*

DNA and RNA can also form hybrid structures (i.e., structures comprising both nucleic acids) that play roles in transcription regulation and serve as intermediates for more complex formations such as triplex structures, which are significant regulators of gene expression.[10]

## 1.2. Hybrid and Complex Nucleic Acid Structures in Gene Regulation

### 1.2.1. DNA-RNA Hybrids and Triplex Structures

Nucleic acids can form hybrid geometries that are pivotal to transcriptional regulation and genome maintenance, the collective set of cellular processes that preserve DNA integrity, repair damage, and ensure the faithful transmission of genetic information. R-loops, for example, arise during transcription when the nascent RNA strand hybridizes with its complementary DNA sequence, displacing the non-template DNA strand in the duplex. These structures are enriched in promoter and terminator regions, where they influence chromatin accessibility and co-transcriptional processes. While transient under normal conditions, persistent R-loops are linked to replication stress, DNA damage, and genomic instability, highlighting the necessity of their precise regulation.[11]

Besides R-loops, hybrid structures include RNA-DNA duplexes, involved in transcriptional interference and gene silencing, and RNA-DNA-RNA hybrids, implicated in regulatory networks driven by non-coding RNAs. These diverse hybrids underscore the adaptability of nucleic acids in facilitating molecular interactions and serve as intermediates to more complex structures, such as triplexes.[12]

Figure 8 illustrates nucleic acid structures with distinct properties. Panel A highlights the triplex DNA structure, which is formed through the sequence-dependent binding of DNA or RNA fragments, referred to as triplex-forming oligonucleotides (TFOs), to the double-helix DNA. Panel B depicts a cruciform DNA structure, arising from inverted repeat sequences. These inverted repeats fold into a stem-loop conformation, with the loop size determined by the length of the sequence gap between the repeats.

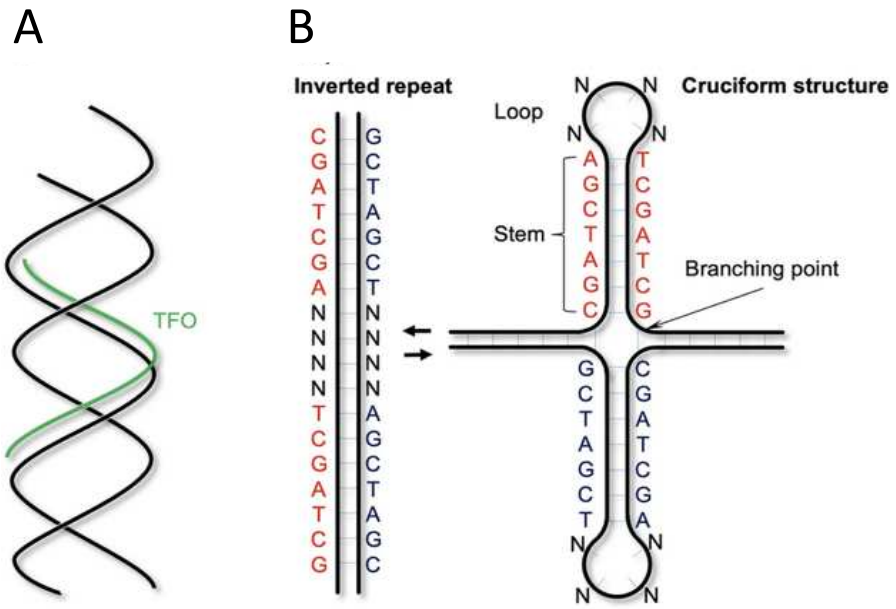


*Figure 8: (A) Triplex formed by sequence-specific binding of triplex-forming oligonucleotides (TFO) to double-helix DNA. (B) Cruciform DNA arising from inverted repeats, with stability influenced by loop size and sequence Reproduced from ref. [12]*

## 1.2.2. Mechanisms of Triplex Formation

Triplex nucleic acids, hypothesized, among others, by Alexander Rich and colleagues in 1957 [13], [14] and experimentally confirmed in the 1980s [15], represent a significant milestone in understanding alternative nucleic acid structures. These triple-helical formations occur when a third strand binds to the major groove of double-stranded DNA (dsDNA), specifically targeting homopurine-homopyrimidine sequences. The third strand interacts through Hoogsteen or reverse Hoogsteen hydrogen bonding, resulting in characteristic triplet structures such as T·AT and C·GC, where the dot represents the Hoogsteen or reverse Hoogsteen bond.[16]

Triplexes are classified based on the orientation of the third strand relative to the DNA duplex and the chemical composition of the third strand. In parallel triplexes, the third strand aligns in the same 5'->3' direction as the purine-rich strand of the DNA duplex, while in antiparallel triplexes, the third strand binds in the opposite orientation.[15], [16]

Additionally, triplexes are further categorized into pyrimidine motif and purine motif triplexes. Pyrimidine motif triplexes comprise a third strand rich in cytosine and thymine, which pairs with the homopurine strand of the duplex via Hoogsteen hydrogen bonds,

often requiring acidic conditions to stabilize protonated cytosines.[17] In contrast, purine motif triplexes comprise a third strand composed of purines (adenine and guanine), which binds to the homopurine strand of the duplex via reverse Hoogsteen hydrogen bonds, forming a more stable structure under physiological conditions.[18]

Figure 9 shows the structural features of TFOs. Panel A illustrates parallel triplexes stabilized by Hoogsteen hydrogen bonds (light blue), while Panel B depicts antiparallel triplexes stabilized by reverse Hoogsteen hydrogen bonds (light green).

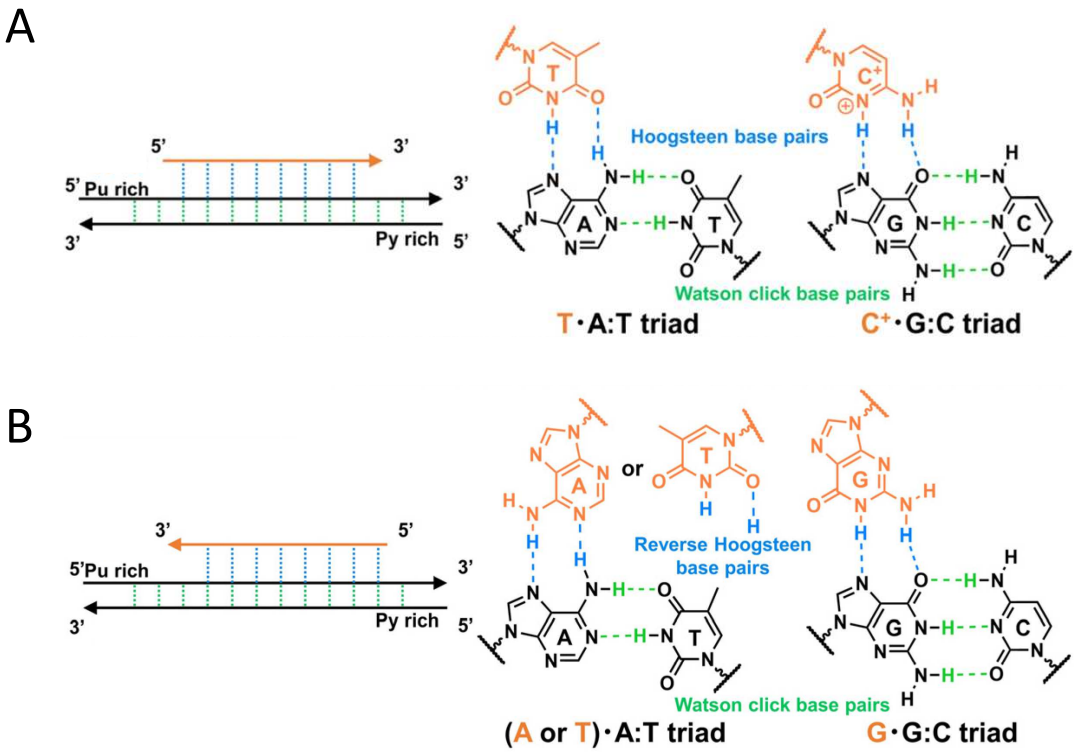


*Figure 9: Panel (A): Parallel triplexes formed via Hoogsteen bonds (blue). Panel (B): Antiparallel triplexes formed via reverse Hoogsteen bonds (green).[69]*

The stability and formation of triplexes is affected by several factors, including sequence specificity, pH, ionic strength, and the presence of stabilizing cations such as potassium and magnesium.[5], [15]

These conditions modulate the structural integrity of triplexes, particularly in dynamic cellular environments.[16]

Once formed, triplexes, often found at regulatory DNA regions such as promoters, enhancers, or telomeres, they influence chromatin architecture and protein binding.[19] These structures act as scaffolds for interactions with nucleic acids and proteins, enabling

precise modulation of transcriptional activity and chromatin organization. Their functional implications extend beyond transcriptional regulation, as detailed in the following section.

### 1.2.3. Functional Roles of DNA-RNA Triplexes in Gene Expression

It has been proposed that DNA-RNA triplexes play critical roles in the regulation of gene expression, acting as versatile modulators of transcription and chromatin dynamics. By their specific formation at specific genomic regions, triplexes influence the accessibility of regulatory elements, thereby controlling the initiation and progression of transcription. They can inhibit transcription by sterically hindering RNA polymerase or transcription factor binding. Conversely, triplexes can enhance transcription by recruiting chromatin remodelers and epigenetic enzymes, such as histone acetyltransferases (HATs) and methyltransferases (HMTs), to establish transcriptionally active chromatin states.[16], [20], [21]

Chromatin remodeling refers to the dynamic modification of chromatin structure to regulate DNA accessibility for transcription.[22] This process is mediated by chromatin remodeler proteins, which reposition, eject, or restructure nucleosomes, thereby modulating transcriptional activity.[23] DNA-RNA triplexes influence chromatin remodeling by recruiting specific remodelers to key regulatory regions.

Histone acetyltransferases (HATs) catalyze the addition of acetyl groups to lysine residues on histone tails, reducing histone-DNA interactions and promoting transcriptional activation. For example, the HAT enzyme GCN5 is known to facilitate transcriptional initiation by creating a more relaxed chromatin state.[24] In contrast, histone methyltransferases (HMTs) like EZH2 deposit methyl groups on histone tails, leading to transcriptional repression or activation depending on the context and specific lysine residue targeted. These enzymes work in concert to fine-tune chromatin states in response to cellular and environmental cues.[25]

Triplex-mediated chromatin remodeling also impacts nucleosome positioning and histone modifications, which regulate DNA accessibility and transcriptional activity.[4], [21]

These structures contribute to maintaining genomic stability by stabilizing regions prone to DNA damage or replication stress, facilitating repair and recombination through the

recruitment of repair proteins. This protective role highlights their importance in safeguarding genetic information under conditions of cellular stress.[26], [27]

The functional versatility of triplexes highlights their significance in transcriptional regulation, chromatin organization, and genome maintenance. These mechanisms, including chromatin remodeling and epigenetic modifications, are predominantly associated with eukaryotic cells, where complex regulatory networks govern gene expression. In contrast, bacterial systems provide a simplified yet informative model to study fundamental aspects of gene regulation. Their relatively straightforward transcriptional and translational processes allow for a clearer investigation of triplex dynamics without the complexities of chromatin-associated factors. Despite these differences, insights gained from bacterial models can serve as a foundation for understanding triplex-mediated regulation in more complex organisms, offering a scalable approach to studying gene expression mechanisms across different biological systems.

## 1.3. Gene Expression and Regulation in Bacteria

Gene expression in bacteria is a highly coordinated process that enables cells to respond rapidly to environmental changes and maintain cellular homeostasis. It involves the conversion of genetic information stored in DNA into functional RNA and proteins through the tightly regulated steps of transcription and translation. Regulation at the transcriptional level is particularly crucial, as it dictates the quantity and timing of RNA synthesis, ensuring that genes are expressed in response to cellular demands. This precise control allows bacteria to adapt their gene expression profiles to varying conditions such as nutrient availability, temperature shifts, and stress factors.[26], [27]

The regulation of bacterial gene expression integrates multiple layers of control, from transcription initiation to RNA processing and degradation. Key regulatory elements include sigma/transcription factors that bind to promoter sequences and driving the RNA polymerase complex, dictating which genes are expressed. Post-transcriptional mechanisms, such as the influence of small regulatory RNAs, also contribute to the fine-tuning of gene expression, enabling bacteria to optimize their growth and survival in diverse environments.[27], [28]

### 1.3.1. Transcription and Translation Regulation Mechanisms

In bacteria, gene expression is driven by efficient transcription and translation processes that enable rapid adaptation to environmental changes. The initiation of transcription, the first step in gene expression, is a highly regulated process in bacteria and involves precise recognition of promoter sequences by RNA polymerase (RNAp). RNA polymerase is a multi-subunit enzyme composed of β, β', two α subunits, and a small ω subunit. While this core enzyme catalyzes the synthesis of RNA complementary to the DNA template strand, it cannot initiate transcription independently. The addition of a sigma factor transforms the core enzyme into the RNA polymerase holoenzyme, capable of recognizing specific promoter sequences and initiating transcription at the correct site. Sigma factors are essential for promoter recognition, unwinding of DNA, and recruitment of transcription activators to initiate transcription efficiently.[29], [30]

In *Escherichia coli*, a model organism for transcriptional studies, the primary sigma factor is σ70, which governs the transcription of housekeeping genes. Additional alternative sigma factors regulate gene expression under specific environmental conditions or stress responses, enabling the bacterium to adapt to various challenges. Each sigma factor binds to a specific class of promoters with conserved sequences at -35 (TTGACA) and -10 (TATAAT) positions relative to the transcription start site (TSS) at +1. The spacer between these elements is crucial for promoter activity and sigma factor binding. Once the RNAp holoenzyme binds the promoter, transcription proceeds in the 5' to 3' direction, synthesizing mRNA until a termination signal is reached.[31], [32]

Termination of transcription occurs via two primary mechanisms: intrinsic termination, where an RNA hairpin structure followed by a poly-uracil sequence causes RNAp to detach, or Rho-dependent termination, where the Rho protein unwinds the RNA-DNA hybrid, releasing the transcript.[33], [34]

Figure 10 provides a schematic representation of the RNA polymerase holoenzyme assembly. The sigma factor associates with the RNA polymerase core enzyme to form the holoenzyme, enabling the recognition and binding of promoter sequences. This interaction is critical for the initiation of transcription at the appropriate site, ensuring accurate gene expression regulation.

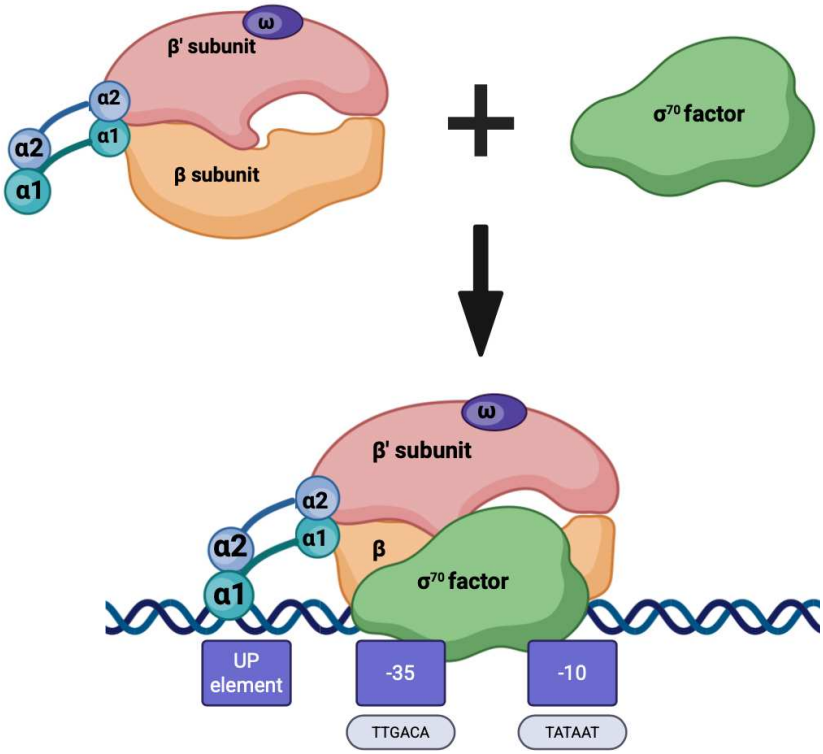


*Figure 10: RNAp holoenzyme consist of sigma factor and binding into promotor region of the DNA. Created with BioRender*

Translation in bacteria begins concurrently with transcription, as ribosomes initiate protein synthesis on nascent mRNA transcripts. The ribosome binding site (Shine-Dalgarno sequence) upstream of the start codon ensures alignment of the mRNA with the ribosome. The ribosome decodes the mRNA sequence into a polypeptide, adding amino acids sequentially as directed by the codons. Translation elongation is energy-intensive, requiring GTP for tRNA movement and peptide bond formation. The process concludes when a stop codon is encountered, releasing the completed polypeptide and dissociating the ribosome-mRNA complex. This coupling of transcription and translation allows bacterial cells to optimize gene expression and respond dynamically to changing environments.[27], [35]

### 1.3.2. Regulatory Roles of Long Non-Coding RNAs

Non-coding RNAs (ncRNAs) are a diverse class of RNA molecules that do not encode proteins but play pivotal regulatory roles in cellular processes. They are broadly categorized into two groups based on their length: small non-coding RNAs (sncRNAs), typically under

200 nucleotides, and long non-coding RNAs (lncRNAs), which are longer than 200 nucleotides. Examples of sncRNAs include microRNAs (miRNAs) and small interfering RNAs (siRNAs), which are well-studied for their roles in RNA silencing and post-transcriptional regulation. Other classes of ncRNAs include circular RNAs (circRNAs), transfer RNAs (tRNAs), and ribosomal RNAs (rRNAs), which participate in fundamental cellular activities. The versatility of ncRNAs highlights their significance in gene regulation, with lncRNAs standing out as dynamic regulators of gene expression in eukaryotic systems.[36], [37]

Long non-coding RNAs (lncRNAs) are involved in regulating both transcriptional and post-transcriptional processes. Unlike small regulatory RNAs found in bacterial systems, such as small RNAs (sRNAs) that modulate transcription termination, mRNA stability, and translation efficiency, lncRNAs predominantly operate in eukaryotic systems and exhibit more complex regulatory mechanisms. [36], [37]

lncRNAs can act as antisense RNAs, pairing with complementary sequences in mRNAs to stabilize transcripts or promote their degradation. Certain lncRNAs recruit RNA-binding proteins (RBPs) that can either enhance mRNA stability or facilitate its decay, providing a mechanism for fine-tuning gene expression. This dual functionality enables lncRNAs to regulate protein synthesis in response to cellular stimuli.

In addition to their post-transcriptional roles, lncRNAs influence transcriptional activity by interacting with transcription factors, chromatin-modifying complexes, and DNA itself. lncRNAs can form DNA-RNA hybrid structures, such as R-loops or triplexes, that modulate chromatin accessibility. These hybrid structures regulate transcription by facilitating or hindering the recruitment of transcriptional machinery to specific regions of the genome.[38], [39]

## 1.4. Role of Polyamines in Nucleic Acid Dynamics

Polyamines are small, positively charged organic molecules that regulate nucleic acid dynamics, a term referring to the structural flexibility, folding, and interactions of DNA and RNA, which are essential for replication, transcription, translation, and chromatin organization. By interacting electrostatically with the negatively charged phosphate backbones of nucleic acids, polyamines stabilize their structures and modulate biological functions, including transcriptional regulation and chromatin remodeling.[40], [41], [42]

### 1.4.1. Discovery and Biological Roles of Polyamines

The biological significance of polyamines was first recognized in the late 17th century by Antoni van Leeuwenhoek, who observed spermine crystals in human semen. Subsequent research in the 20th century identified their roles in cellular growth, nucleic acid stabilization, and chromatin organization. The primary polyamines in eukaryotic cells—putrescine (1,4-diaminobutane), spermidine (N-(3-aminopropyl)-1,4-diaminobutane), and spermine (N,N'-bis(3-aminopropyl)-1,4-diaminobutane)—are synthesized from ornithine and methionine via tightly regulated enzymatic pathways. In addition, cadaverine (1,5-diaminopentane), derived from lysine decarboxylation, is another biologically significant polyamine.[43], [44]

Polyamines stabilize nucleic acids by neutralizing their negative charges, reducing electrostatic repulsion, and enhancing structural integrity. They regulate transcription and translation by modulating chromatin accessibility and ribosome assembly, ensuring efficient gene expression.[41], [42] During oxidative stress, polyamines neutralize reactive oxygen species (ROS), protecting cellular membranes and organelles from damage. They also play a key role in chromatin remodeling by influencing nucleosome positioning and histone modifications, thereby enabling precise transcriptional regulation.[43], [45], [46] Dysregulation of polyamine metabolism has been associated with pathological states such as cancer, neurodegenerative disorders, and inflammatory diseases, highlighting their importance in cellular homeostasis.[46], [47]

### 1.4.2. Influence of Polyamines on Nucleic Acid Structures

The stabilizing properties of polyamines on nucleic acids were first described in the mid-20th century. Studies showed that polyamines neutralize the negative charges of DNA and RNA backbones, reducing electrostatic repulsion and enhancing structural stability.[41], [48] They stabilize double-stranded DNA (dsDNA), support chromatin compaction, and ensure the conformational stability of RNA molecules, including ribosomal RNA (rRNA), which is critical for translation fidelity and ribosome assembly.[45], [48] Polyamines are also involved in the formation and stabilization of non-canonical DNA structures, such as Z-DNA (i.e., a lefthanded DNA double-helix geometry) and triplex DNA, which play roles in transcriptional regulation and recombination. In the context of triplex DNA, polyamines

neutralize the phosphodiester backbones of all three strands, enhancing stability and allowing triplexes to modulate transcription, chromatin accessibility, and epigenetic modifications.[44], [48]

Studies demonstrate that polyamines promote triplex formation under physiological conditions, linking them to transcriptional regulation and chromatin remodeling.[49], [50] These effects highlight the critical role of polyamines in maintaining nucleic acid dynamics and regulating cellular processes. Their influence extends from nucleic acid stabilization to transcriptional control, bridging their structural and functional contributions to gene expression and chromatin organization.

## 1.5. Triplex Applications in Synthetic Biology Research

Synthetic biology is a recently developed interdisciplinary scientific field that investigates biological systems that do not occur naturally. The European Union provides the following definitions: “Engineering of biological components and systems that do not exist in nature, and the re-engineering of existing biological systems; it is determined on the intentional design of artificial systems, rather than an understanding of natural biology” (*Synthetic Biology project* EU FP631). Additionally, synthetic biology is described as “the application of science, technology, and engineering to facilitate and accelerate the design, manufacture and/or modification of genetic materials in living organisms” (European Commission, *Opinion on Synthetic Biology* I Definition, SCHER, SCENIHR, SCCS). This field provides tools for controlling transcriptional processes and regulating gene expression with precision.[51]

Synthetic biology offers a precise framework for studying the structural and functional aspects of triplex DNA. By engineering artificial biological components, researchers can evaluate the role of triplex-forming oligonucleotides (TFOs) and their interactions with double-stranded DNA (dsDNA) to regulate transcription and chromatin remodeling. These approaches enable the design of synthetic constructs that model triplex-mediated regulatory processes, providing insights into their impact on gene expression.[52]

### 1.5.1. Synthetic Genelet Systems for Triplex Analysis

A pioneering synthetic biology tool for investigating triplex DNA is the genelet system, a modular DNA construct designed to mimic transcriptional processes in vitro. Genelets consist of a duplex DNA template with a partially single-stranded promoter region. In the "OFF" state, this promoter exhibits low affinity for transcriptional machinery, such as the T7 RNA polymerase (T7 RNAp). Upon addition of complementary single-stranded DNA (ssDNA), the promoter transitions to an "ON" state, forming a full duplex that enables efficient T7 RNAp binding and transcription initiation. This tool has been used effectively to explore how synthetic DNA-RNA triplexes modulate transcriptional activity under controlled conditions.[53]

Figure 11 illustrates a general scheme of the genelet system. The mechanism involves a synthetic duplex DNA template with a partially single-stranded promoter region and the T7 RNAp enzyme. In the “OFF” state, RNAp exhibits low affinity for the single-stranded promoter, resulting in very slow transcription.[54] Upon the addition of sequence-specific ssDNA to the promoter, the single-stranded region is converted into a complete duplex promoter. This conformational change allows RNAp to bind with high affinity and catalyze RNA transcription at a faster rate. The activity of the genelet can be monitored through quantification of RNA production or by fluorescence emission from a fluorophore-quencher pair positioned at the promoter’s end, labeled as F (fluorophore) and Q (quencher) in the figure.

Genelet systems were adapted for investigating how triplex-forming oligonucleotides (TFO) influence transcription, introducing a triplex-duplex transition instead of the single strand-duplex transition. By integrating TFOs into the promoter region, researchers can assess their effects on transcription rates and gene regulation. These systems mimic natural transcriptional processes, offering valuable insights into triplex dynamics under controlled conditions. Triplex-operated genelets also allow for the study of stabilizing agents, such as polyamines, and their ability to enhance triplex stability and functionality in regulatory contexts.[55]

Beyond single transcription units, complex interoperating genelet circuits have been programmed for the creation of molecular neural networks. However, one limitation of the approach is the instability of single-stranded nucleic acids in cellular environments, restricting the use of genelets in vivo.[56][54]

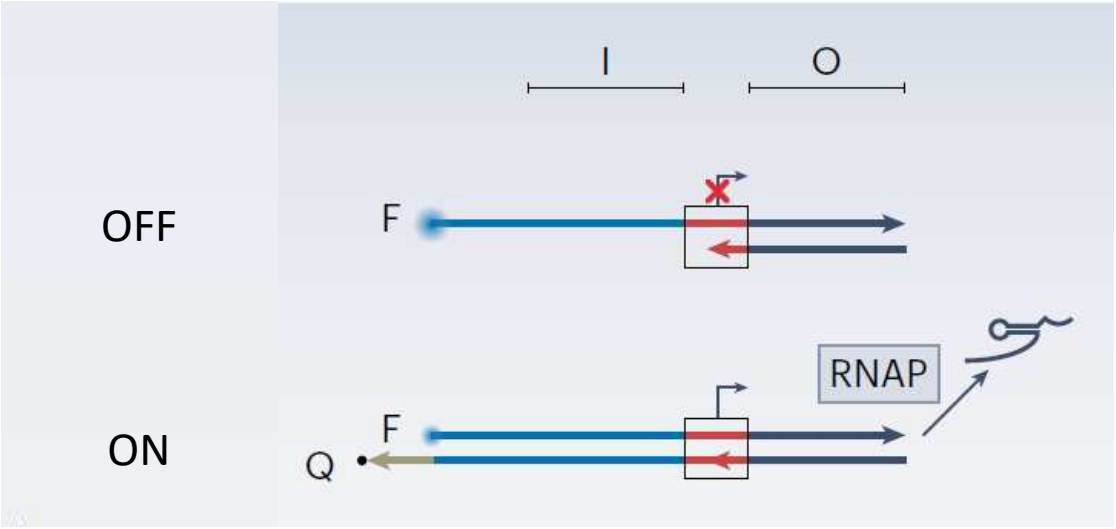


Figure 11: Scheme of the genelet system showing regulation via switching between a single-stranded promoter (OFF state) and a double-stranded promoter (ON state). Q represents the quencher, and F represents the fluorophore. Reproduced with modifications from ref.[70]

### 1.5.2. RNA-DNA Hybrid Triplex Research

Synthetic biology provides tools to explore RNA-DNA hybrid triplexes, particularly in the context of long non-coding RNAs (lncRNAs). Growing evidence is pointing at lncRNAs interacting with chromatin and form RNA-DNA triplexes, which contribute to transcriptional regulation and chromatin remodeling. By using modular synthetic systems, researchers can replicate these interactions *in vitro*, offering a simplified yet controlled environment for studying lncRNA functions.

Engineered transcriptional units that mimic lncRNA functions can be used to produce RNA molecules capable of forming hybrid triplexes with dsDNA. These synthetic approaches provide direct insights into RNA-DNA interactions and their role in gene expression. This capability is particularly useful for dissecting the regulatory functions of lncRNAs in chromatin architecture and transcriptional activity.[57]

### 1.5.3. Therapeutic Potential of Synthetic Triplex Systems

Synthetic biology enables the development of triplex-based therapeutic strategies targeting disease-related genes. Engineered TFOs can modulate transcription by silencing oncogenes, activating tumour suppressor genes, or preventing transcription of essential

viral genes. Triplex systems have also been explored as delivery platforms for nucleic acid-based therapeutics, improving their specificity and stability *in vivo*.

By leveraging synthetic biology, these therapeutic approaches can be optimized to achieve precise regulation of gene expression in disease contexts. For example, triplex systems are being evaluated for their potential in cancer gene therapy and antiviral treatments, demonstrating their value in advancing personalized medicine and precision therapeutics.[58]

## 1.6. Analytical and Biological Approaches to Study Triplexes

The study of triplex-mediated effects on gene expression requires a combination of analytical and functional techniques to evaluate their formation, stability, and potential regulatory roles. Key methods used in this research include electrophoretic mobility shift assays (EMSA) to detect triplex formation, temperature-dependent denaturation analysis to assess thermal stability, and mass spectrometry to validate the molecular composition and stoichiometry of triplex structures. Computational modelling was employed to investigate spermine stabilizing interactions with triplexes, while *in vitro* transcription-translation experiments evaluated the downstream effects of triplex formation on protein synthesis. These complementary approaches form a robust framework for understanding the biological significance of triplexes and their stabilization by polyamines.[59], [60], [61]

# 2. Aim of the Study

This thesis investigated the role of polyamines—spermine, spermidine, cadaverine, and putrescine—in the formation and stability of Hoogsteen-stabilized hybrid DNA-RNA triplex structures.

Polyamines are known to bind to polyanionic chemical species in cells, including DNA and RNA. They stabilize nucleic acid secondary structures, and this study explores their ability to modulate hybrid RNA-DNA triplex formation under controlled *in vitro* conditions, designed to approximate physiological environments. Previous findings demonstrated how designed-sequence triplexes could up- or down-regulate transcription rates from bacterial transcription units *in vitro*, in the presence of high concentrations of magnesium. Based on those results, this research evaluated whether polyamine-mediated stabilization could replace metal ions to counter-balance electrostatic repulsion in the triplex complex.

By employing biophysical and biochemical approaches, this work characterized the binding stability of triplex structures in the presence of polyamines. Electrophoretic mobility shift assay (EMSA) and temperature-dependent triplex denaturation (Tm) analysis were used to detect triplex formation and measured these structures thermal stability. Specifically, dissociation constants ($K_d$) were obtained from comparing duplex/triplex ratios at different polyamine concentrations, and these parameters were used to evaluate complex stability. In addition, mass spectrometry analysis and molecular modelling cross-validated the molecular composition and stoichiometry of the analysed triplexes.

Furthermore, the downstream effects of triplex formation on transcriptional and translational regulation and protein expression were analyzed to elucidate the mechanisms by which polyamines impact these processes. *In vitro* transcription-translation experiments were performed to assess how triplex stabilization by spermine modulates transcriptional and translational outputs in the context of bacterial promoters, providing direct insights into their effects on protein biosynthesis.

The final goal of this research is to determine whether polyamines affect transcription by stabilizing duplex-associated RNA (i.e., triplexes) formed at regulatory genomic regions, such as promoters. By integrating thermodynamic and structural analyses, this thesis provides novel insights into how triplex nucleic acid-mediated polyamines might contribute to gene regulation, potentially uncovering an unexplored mechanism involving polyamines and transcriptional control. Considering how polyamine metabolism is dysregulated in

some tumours, these results could be used to explore new anti-tumour approaches in the context of RNA-based therapies.

# 3. MATERIALS AND METHODS

In this section, chemicals and instruments used in this study, as well as methodologies and protocols for the thermodynamic characterization of triplexes, including EMSA, and mass spectroscopy, molecular modelling and *in vitro* transcription-translation are described.

## 3.1. Materials

In this section, the list of reagents, nucleic acid sequences, and instruments utilised in this study are reported.

### 3.1.1. Reagents and Chemicals

All nucleic acid sequences of TTSs and TFOs are reported in Tables 1 and 2, respectively, and were purchased from IDT (Integrated DNA Technologies, Coralville, Iowa, USA) as freeze-dried powder, dissolved as stock solutions in ultrapure water upon arrival, and stored at -20°C for further use. Transcription units TU1 and TU2 (Table 3) were ordered as freeze-dried duplexes from Twist Bioscience (USA). All solutions were prepared using ultrapure water from a Genie Direct-Pure water device (RephiLe Bioscience Ltd., China), with a resistivity of 18.0 MΩ·cm.

Acetic acid was purchased from Janssen Pharmaceuticals. 30% acrylamide/bis-acrylamide 19:1 solution, ammonium persulfate (APS), N,N,N',N'-tetramethylethylenediamine (TEMED), TBE 5X (Tris/Borate/EDTA), bromophenol blue, and glycerol were purchased from Merck, Darmstadt, Germany.

NEBExpress® Cell-free *E. coli* Protein Synthesis System, RNase inhibitors, and Protein Synthesis Buffer, was purchased from New England Biolabs (NEB, USA) and used for the in vitro transcription-translation experiments.

*In vitro* transcription-translation experiments were carried out with excitation 433 nm and emission was collected at 475 nm.

Nucleic acid stains oxazole gold and thiazole green were purchased from Biotium Inc. (San Francisco, California, USA). Additionally, HCl and NaOH were purchased from Merck, Darmstadt, Germany and were used for pH adjusting.

Tris HCl was purchased from Avantor, Radnor, Pennsylvania, USA as dried basis; dithiothreitol (DTT) was purchased from AppliChem GmbH, Germany; Triton X-100 and $MgCl_2$ were purchased from Merck, Darmstadt, Germany.

Temperature-dependent melting curve experiments were carried out with excitation at 498 nm and emission at 522 nm.

N'-(3-aminopropyl)butane-1,4-diamine;trihydrochloride (Spermidine) with ≥99% purity was purchased from Fluka (Sigma-Aldrich, Buchs, Switzerland). 1,5-Diaminopentane (Cadaverine) with 95% purity, 1,4-Butanediamine dihydrochloride (Putrescine dihydrochloride) with ≥98% purity and N,N'-Bis(3-aminopropyl)-1,4-butanediamine tetrahydrochloride (spermine tetrahydrochloride) with ≥98% purity were all purchased from Sigma-Aldrich (Buchs, Switzerland).

Sample buffer for mass analysis was prepared with ammonium acetate (≥99% purity, Merck, Darmstadt, Germany) dissolved in water and supplemented with 10% isopropanol (≥99.9% purity, Merck, Darmstadt, Germany).

*Table 1: Sense and antisense triplex target site (TTS) DNA sequences.*

| **TTS Name** | **Sequence** |
|---|---|
| TTS SENSE | 5'- TCC TCT TCT CCT CCT -3' |
| TTS ANTI SENSE | 5'- AGG AGG AGA AGA GGA – 3' |

*Table 2: Triplex-forming oligonucleotide (TFO) RNA sequences.*

| **TFO Name** | **Sequence** |
|---|---|
| TFO1 | 5'- UCC UCC UCU UCU CCU- 3' |
| TFO2 | 5'- AGG AGA AGA GGA GGA – 3' |

*Table 3: Transcription unit sequences, TU1 and TU2, used for In vitro* transcription-translation experiments.

| Sequence name | Sequence - only the (+) strand is reported |
|---|---|
| TU1 with TTS | **5'-** TTG ACA GGA GGA GAA GAG GAT ATA ATA GGA GGA GAA GAG GAA AGG AGA AAA AAA AAT GAA TCA CAA AGT GGT GAG CAA GGG CGA GGA GCT GTT CAC CGG GGT GGT GCC CAT CCT GGT CGA GCT GGA CGG CGA CGT AAA CGG CCA CAG GTT CAG CGT GTC CGG CGA GGG CGA GGG CGA TGC CAC CTA CGG CAA GCT GAC CCT GAA GTT CAT CTG CAC CAC CGG CAA GCT GCC CGT GCC CTG GCC CAC CCT CGT GAC CAC CCT GAC CTG GGG CGT GCA GTG CTT CGC CCG CTA CCC CGA CCA CAT GAA GCA GCA CGA CTT CTT CAA GTC CGC CAT GCC CGA AGG CTA CGT CCA GGA GCG TAC CAT CTT CTT CAA GGA CGA CGG CAA CTA CAA GAC CCG CGC CGA GGT GAA GTT CGA GGG CGA CAC CCT GGT GAA CCG CAT CGA GCT GAA GGG CAT CGA CTT CAA GGA GGA CGG CAA CAT CCT GGG GCA CAA GCT GGA GTA CAA CGC CAT CAG CGA CAA CGT CTA TAT CAC CGC CGA CAA GCA GAA GAA CGG CAT CAA GGC CCA CTT CAA GAT CCG CCA CAA CAT CGA GGA CGG CAG CGT GCA GCT CGC CGA CCA CTA CCA GCA GAA CAC CCC CAT CGG CGA CGG CCC CGT GCT GCT GCC CGA CAA CCA CTA CCT GAG CAC CCA GTC CAA GCT GAG CAA AGA CCC CAA CGA GAA GCG CGA TCA CAT GGT CCT GCT GGA GTT CGT GAC CGC CGC CGG GAT CAC TCT CGG CAT GGA CGA GCT GTA CAA GTA GTA AT**-3'** |
| TU2 w/o TTS | **5'-** TTG ACA ATT AAT TCA TCC GGC TCG TAT AAT GTG TGG AAG GAG AAA AAA AAAT GAA TCA CAA AGT GGT GAG CAA GGG CGA GGA GCT GTT CAC CGG GGT GGT GCC CAT CCT GGT CGA GCT GGA CGG CGA CGT AAA CGG CCA CAG GTT CAG CGT GTC CGG CGA GGG CGA GGG CGA TGC CAC CTA CGG CAA GCT GAC CCT GAA GTT CAT CTG CAC CAC CGG CAA GCT GCC CGT GCC CTG GCC CAC CCT CGT GAC CAC CCT GAC CTG GGG CGT GCA GTG CTT CGC CCG CTA CCC CGA CCA CAT GAA GCA GCA CGA CTT CTT CAA GTC CGC CAT GCC CGA AGG CTA CGT CCA GGA GCG TAC CAT CTT CTT CAA GGA CGA CGG CAA CTA CAA GAC CCG CGC CGA GGT GAA GTT CGA GGG CGA CAC CCT GGT GAA CCG CAT CGA GCT GAA GGG CAT CGA CTT CAA GGA GGA CGG CAA CAT CCT GGG GCA CAA GCT GGA GTA CAA CGC CAT CAG CGA CAA CGT CTA TAT CAC CGC CGA CAA GCA GAA GAA CGG CAT CAA GGC CCA CTT CAA GAT CCG CCA CAA CAT CGA GGA CGG CAG CGT GCA GCT CGC CGA CCA CTA CCA GCA GAA CAC CCC CAT CGG CGA CGG CCC CGT GCT GCT GCC CGA CAA CCA CTA CCT GAG CAC CCA GTC CAA GCT GAG CAA AGA CCC CAA CGA GAA GCG CGA TCA CAT GGT CCT GCT GGA GTT CGT GAC CGC CGC CGG GAT CAC TCT CGG CAT GGA CGA GCT GTA CAA GTA GTA T**-3'** |

### 3.1.2. Instruments

A thermal cycler (Applied Biosystems, Waltham, Massachusetts, USA) was used for double-strand DNA annealing procedure. Samples were centrifuged using Eppendorf centrifuge 5810 R (Eppendorf Inc., Germany). The pH was adjusted using a Crison pHmeter Basic $20^{+}$ manufactured by Crison Riera Principal (Spain). Electrophoretic runs were performed in a Mini-PROTEAN Tetra System electrophoresis chamber (BIO-RAD, Hercules, California, USA) connected to a PowerEase Touch 350 W power supply (Invitrogen-ThermoFisher, Waltham, Massachusetts, USA). Electrophoretic gel fluorescence emission images were acquired with an Invitrogen iBright 1500 (Invitrogen-ThermoFisher Scientific, Waltham, Massachusetts, USA).

Fluorescence plate reader CLARIOSTAR+ plate reader (BMG LABTECH) was used for *in vitro* transcription-translation experiments, along with Lumox® 384 multiwell plates (Sarstedt, Germany) and AB-0580 Adhesive Plate Seals from ThermoScientific (Waltham, Massachusetts, USA). An SL 8R Centrifuge (ThermoScientific, Waltham, Massachusetts, USA) was used for microplate centrifugation with a M-10 microplate swinging bucket rotor. A Stratagene Mx3000P (Agilent Technologies, Santa Clara, California, USA) real-time qPCR machine was used for melting temperature experiments along with white-colored qPCR optically clear caps (Thermo-Fisher Scientific Inc., Waltham, Massachusetts, USA).

Mass spectrometry analysis was performed using a 6520 Q-TOF mass spectrometer (Agilent Technologies, Santa Clara, California, USA) equipped with a Chip Cube nano-ESI interface. The instrument operated in high-resolution mode (R = 10,000) with negative polarity. Nitrogen was used as the desolvating gas, maintained at 40 °C with a flow rate of 8 L/min.

ORIGINPRO 2018B (OriginLab Corp., Northampton, Massachusetts, USA) software was used to produce all data analyses, including statistical and graphical representations.

## 3.2. Experimental Methods

In this section, protocols and procedures used sequence design, nucleic acid structure characterization, including electrophoretic mobility shift assay (EMSA), temperature-dependent triplex denaturation analysis, molecular modelling, mass analysis, and analysis of *in vitro* transcription-translation are reported.

### 3.2.1. Sequence Design

DNA and RNA sequences from previous studies were used to assemble the hybrid triplexes in this thesis. Specifically, the TTS and TFO sequences used in this thesis were taken from Cecconello et al.[62] where they were originally designed to work as triplex components in a high-$Mg^{2+}$ concentration environment. The sequences are reported in Tables 1 and 2. Figure 12 shows schematically the single-strand components, the duplex assembly, and the triplex assembly, according to Watson-Crick and Hoogsteen base-pair rules.

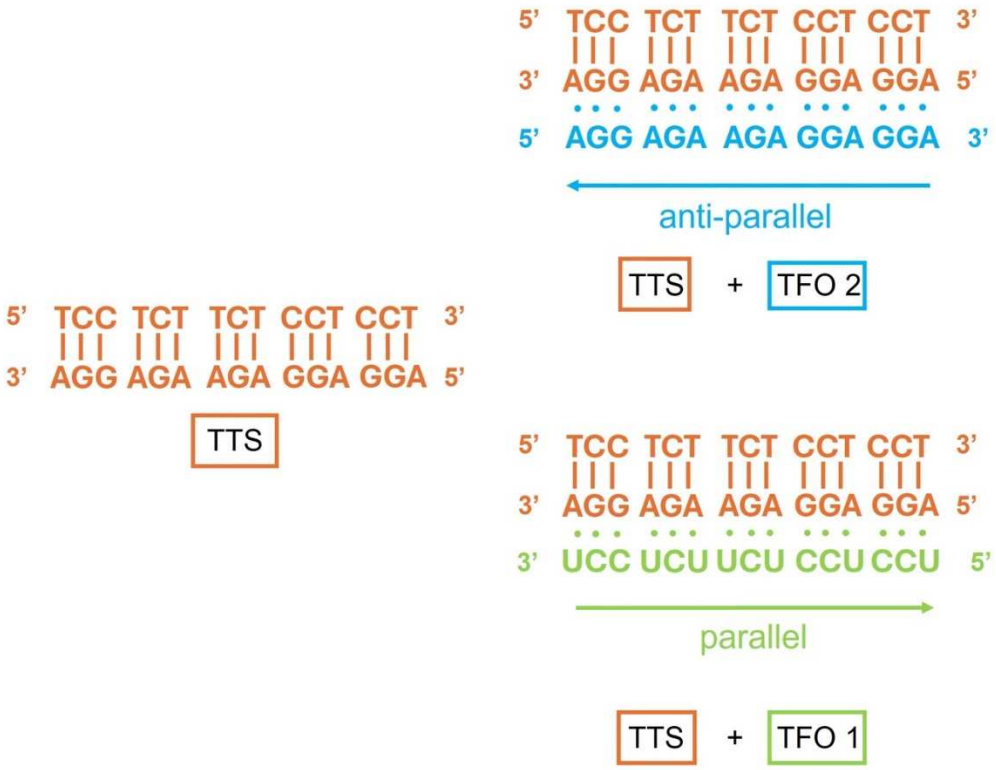


*Figure 12: Schematic representation of triplex formation. Orange lines represent Watson-Crick base pairing, while blue dots indicate reverse Hoogsteen base pairing, and green dots highlight Hoogsteen base pairing in triplex structures.*

### 3.2.2. Triplex Denaturation Analysis

Double strand DNA (dsDNA) annealing procedure and sample buffer preparation was carried out as mentioned previously 25 μL samples were prepared using 100 nM of the TTS (see Table 1) in the presence of the specific purine or pyrimidine TFO (see Table 2) at concentrations in the interval 1-$10^4$ nM in 1X buffer (see buffer A composition on page 44). Samples specific compositions, according to each polyamine, were as follows:

- Spermine
  Concentrations in TFO1 samples from 0 to 10 mM.
  Concentrations in TFO2 samples from 0 to 0.1 mM.
  TTS:TFO1 and TTS:TFO2 ratio: 1:2 (100 nM TTS + 200 nM TFO).

- Spermidine
  Concentrations in TFO1 samples from 0 to 10 mM.
  Concentrations in TFO2 samples from 0 to 10 mM.
  TTS:TFO1 and TTS:TFO2 ratio: 1:1 (100 nM TTS + 100 nM TFO1).

- Putrescine
  Concentrations in TFO1 and TFO2 samples from 0 to 30 mM.
  TTS:TFO1 ratio: 1:2 (100 nM TTS + 200 nM TFO1).
  TTS:TFO2 ratio: 1:1 (100 nM TTS + 100 nM TFO2).

- Cadaverine
  Concentrations in TFO1 and TFO2 samples from 0 to 30 mM.
  TTS:TFO1 ratio: 1:2 (100 nM TTS + 200 nM TFO1).
  TTS:TFO2 ratio: 1:1 (100 nM TTS + 100 nM TFO2).

1X buffer (buffer A) described on page 44 was used for all Tm experiments. After a 30-minute incubation at 4°C, 8 µL of ultrapure water, 2 µL of thiazole green 20X solution, and 10 µL of the above-mentioned sample mix were placed in a white-colored qPCR tube with optically transparent caps. Analyses were performed in a Stratagene Mx3000P qPCR machine that measured fluorescence at 498 nm excitation wavelength and 522 nm emission wavelength in a temperature interval equal to 25 $^{o}$C to 95 $^{o}$C.

Figure 15 reports a graphical representation of the triplex and duplex dissociations at increasing temperatures. The red ribbon represents the TFO while dark and light green ribbons represent the TTS ssDNAs. Melting curve analysis graphs will be described further in the following paragraphs.

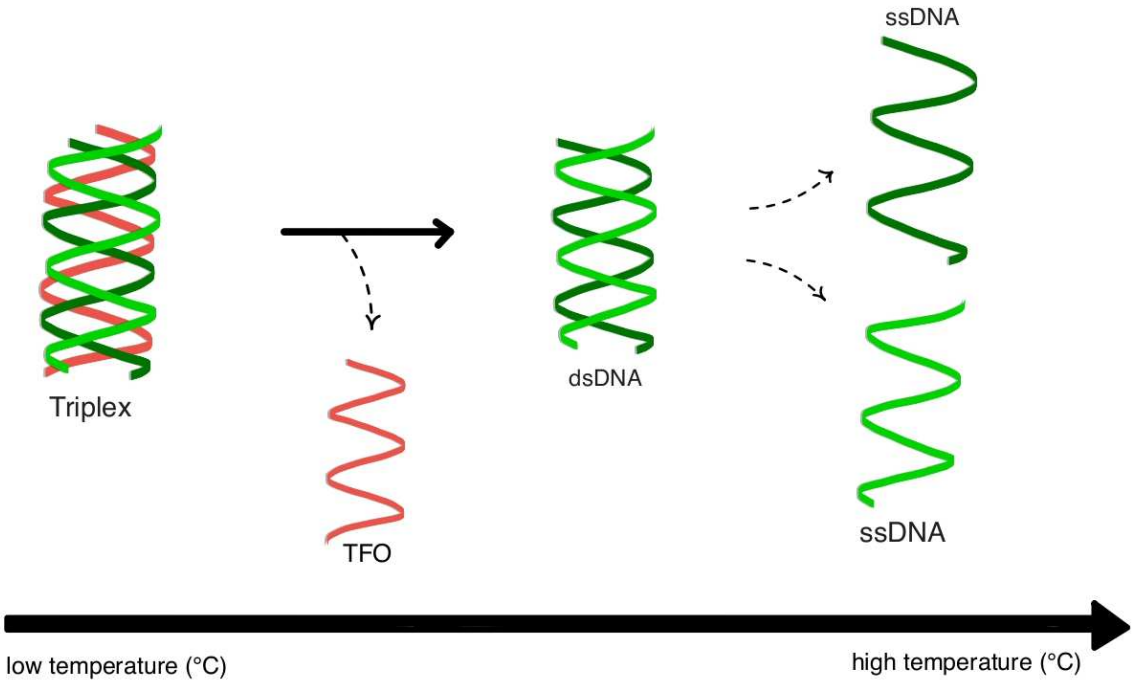


*Figure 13: Schematic representation of the temperature-dependent triplex and duplex dissociation events.*

Thiazole green is a small fluorescent molecule capable of intercalating helical structures of nucleic acids and display an increase of its quantum yield in the nucleic acid-complex state. When thiazole green is free in solution, it is associated with a lower fluorescence quantum yield (QY) compared to the complex-associated QY.

At increasing temperatures, triplex dissociation is promoted as depicted in Figure 10, releasing the TFO in solution, and realizing a decrease in the overall observed thiazole green QY. Hence, a decrease in fluorescence is detected. Similarly, the second decrease in fluorescence occurs due to dsDNA dissociation. When half of the complex is dissociated (i.e., [triplex]=[duplex]), the melting point (Tm) is reached.

To estimate the Tm, the first derivative of the fluorescence changes in respected to temperature, i.e., $-\frac{\Delta F}{\Delta^{\circ}T}$, was plotted against temperature to obtain peaks associated with the strand dissociation events. Two peaks were observed, with intensities proportional to the difference in complex concentration.

To normalize the data, the peak associated with duplex-separation was considered an internal standard, that is, its concentration difference was considered constant for different TFO concentrations. This was used to normalize the triplex peak intensity, with respect to duplex concentration.

In the last step of this analysis, peak intensity ratio:

(Eq. 3) $$Normalized\ peak\ intensity\ ratio = \left(-\frac{\Delta F}{\Delta °T}\right) \text{triplex} \diagup \left(-\frac{\Delta F}{\Delta °T}\right) duplex$$

was plotted against TFO concentration. The estimated dissociation constant value ($K_d$) is given by the TFO concentration at the symmetry point of the sigmoid obtained by fitting the experimental peak intensity ratios with equation (2), for the formula see section 3.2.2.

### 3.2.3. Electrophoretic Mobility Shift Assay (EMSA)

Electrophoretic Mobility Shift Assay (EMSA) Electrophoretic Mobility Shift Assay (EMSA) is a widely used technique for detecting the formation of complexes by changes (shift) in the migration rates of biomolecules in an electrophoretic run. By observing changes in the electrophoretic mobility of biomolecular complexes, EMSA provided evidence of RNA TFO binding to duplex DNA target sequences by Hoogsteen interactions and therefore forming triplexes. This method exploits the slower migration rate of triplex structures compared to other secondary structures including duplex DNA or single strand RNA/DNA strands during gel electrophoresis. For this thesis, EMSA was critical in evaluating TFO binding to duplex DNA and assessing the influence of stabilizing agents, such as polyamines, under controlled conditions. The observed shifts in mobility enabled us to confirm triplex formation and correlate it with regulatory effects on transcription and protein production.[59], [63] In addition, by running samples containing different ratios of duplex DNA/RNA (i.e., TTS/TFO), dissociation constants ($K_d$) were estimated. Specifically, at equilibrium, when duplex and triplex concentrations are identical, $K_d$ is equal to TFO concentration, according to:

$$\text{TFO} + \text{dsDNA} \rightarrow \text{Triplex}$$

(Eq. 1) $$\text{Kd} = \frac{[\text{TFO}][dsDNA]}{[\text{Triplex}]}$$

when [Triplex] = [dsDNA], then Kd = [TFO]

Double-strand DNA (dsDNA) annealing procedure was carried out as follows: 10 μM of sense and antisense complementary strands were placed in a 0.2 mL PCR tube in a 50 mM NaCl aqueous solution. The mixture was placed in a thermocycler and first heated for 5 minutes at 95°C, and then slowly cooled to 4°C at a rate of 2°C $min^{-1}$. The newly formed double-strand DNA solutions were stored at -20 °C until use.

Sample buffer (buffer A) for triplex formation was prepared as a 10X stock solution containing 400 mM Tris HCl, 100 mM $MgCl_2$, 10 mM DTT (dithiothreitol), and 0.1% v/v Triton X-100. The pH was adjusted to 6.9 using concentrated HCl or NaOH solutions and was stored at 4 °C.

Polyacrylamide gels (12% acrylamide/bis-acrylamide 19:1, standard 8x10 cm, ca. 10 mL) were prepared using 6 mL 30% acrylamide/bis-acrylamide 19:1, 3 mL 5X TBE buffer at pH 6.9, 1.5 mL 100 mM $MgCl_2$, 0.5 mL APS 20 mg $mL^{-1}$. The volume to adjusted to 15 mL and 10 μL TEMED were added. The solution was then quickly mixed and poured in the gel caster.

Samples were prepared using 100 nM of the TTS (see Table 1) in the presence of TFO1 or TFO2 (see Table 2) at concentrations in the interval of 1-$10^4$ nM in 1X buffer. Water was added to a final volume equal to 25 μL. After a 30-minute incubation at 4°C, 5 μL of the TTS-TFO mixture, 5 μL of buffer, and 3 μL of loading dye were mixed in a tube at the final volume of 13 μL.

Gel loading dye was prepared using 0.1% bromophenol blue and 50% glycerol, in water.

After the electrophoretic machine was assembled and filled with buffer, it was placed in an ice-cooled bath until it reached thermal equilibrium at 11°C. Samples were then loaded in the gel wells and the electrophoretic separation was started at 75 V, 0.02 A, 1 W, for 2 hours. After separation, gels were stained for 10 minutes in a freshly made 1X oxazole gold staining solution.

Fluorescence images of the gels were acquired with an Invitrogen iBright 1500 imager, through UV excitation. Bands of the gel image were analyzed measuring band intensity via the imager proprietary software. All data were processed using Origin analysis software. The resulting plots were first normalized in the interval 0 – 1 band intensity and then fitted with the following dose-response equation (1).

(Eq. 2) $$y = A1 + \frac{A2 - A1}{1 + 10^{((logx_0) - x)p}}$$

Where x is the logarithm of the TFO concentration, y is the normalized band intensity, A1 and A2 are the left and right asymptotes, respectively, $x_0$ is the TFO concentration at the inflection point (i.e., the dissociation constant, $K_d$), and p is the slope of the sigmoid at the inflection point.

### 3.2.4. Mass Spectrometry

Mass spectrometry was employed to study the binding interactions between DNA/RNA hybrid triplexes and polyamines under controlled conditions. Negative ion ESI mass spectra were recorded for triplex structures and triplex–polyamine complexes. Samples were prepared by mixing DNA duplexes and their corresponding RNA single strands in ammonium acetate buffer (50 mM) supplemented with 10% isopropanol. DNA and RNA were used at final concentrations of 50 µM and 100 µM, respectively, in a total reaction volume of 40 µL. Following a 30-minute incubation at 4 °C to promote triplex formation, the samples were diluted 1:100 with a solution containing 90:10 (v/v) Milli-Q water and isopropanol, buffered with 50 mM ammonium acetate (pH 7.4).

To generate triplex-polyamine complexes, a second incubation at 4 °C was performed with DNA and RNA concentrations of 0.5 µM and 1 µM, respectively, and varying polyamine concentrations. The polyamine binding was assessed under ammonium acetate buffer conditions optimized for detecting triplex-polyamine interactions.

Data analysis focused on distinguishing triplex-associated polyamines from free molecules in solution. Deconvolution of mass signals was conducted using a maximum entropy algorithm, with mass ranges and signal thresholds optimized for resolving hybrid triplex-polyamine complexes.

### 3.2.5. Molecular modelling

Initial triplex structures were obtained with 3D-NuS on-line software (https://iith.ac.in/3dnus/Triplex.html) as pdb files. Simulations were run with the NAMD

2.4 software package.[64] The CHARMM 36 force field has been used to parametrize the interatomic interactions for the RNA and DNA strands, and for the spermine molecules. The latter have been parametrized using the CHARMM-GUI tool [65], while the generalized Born implicit solvent model was used (parameters: alphaCutoff 14 Å, switchdist 15 Å, cutoff 16 Å, ionConcentration 0, solventDielectric 80, pairlistdist 18, sasa off). The initial restraining was imposed to avoid the unfolding of the triplex before the spermine molecules could bind and stabilize the complex.

### 3.2.6. *In Vitro* Transcription-translation

In vitro transcription-translation experiments were conducted to investigate the effect of spermine-stabilized triplex formation on transcriptional and translational efficiency. mCerulean, a bright cyan fluorescent protein with enhanced photostability and brightness (Ex/Em 433/475 nm), was used as the reporter protein to monitor protein biosynthesis in real time.[66]

Two transcription units (TUs) were designed for this study:

TU1: TTS-containing σ70 bacterial promoter + mCerulean fluorescent protein,

TU2: σ70 promoter + mCerulean fluorescent protein.

TU1 included a TTS-modified σ70 bacterial promoter while TU2 consisted in the unmodified σ70 bacterial promoter to test the influence of triplex formation on transcriptional and translational activity.

The first set of samples was prepared to contain 50 nM of the template, 500 nM of the corresponding TFO, spermine concentrations varied depending on the sample (0 , 50, 100, 150, and 200 µM),modified NEB buffer and ultrapure water, for a final volume of 25 µL.

Samples were then incubated at +4°C for 30 minutes. The second set of samples was prepared to contain 3 µL of NEBExpress® Cell-free *E. coli* Protein Synthesis System, protein synthesis buffer 0.5X, 400U/mL of RNAse inhibitors and 5 µL of the first set of samples. These samples were then transferred in a 384-well plate, which was covered with a transparent seal. The plate was loaded in the plate reader, set at 29°C, for an 8-hour fluorescence signal collection in linear shaking conditions. The used excitation wavelength was 433 nm, and the fluorescence signal was filtered at 475 nm. Time-dependent

fluorescence signals were then analyzed using Origin Lab software, where the rates for each sample were fitted linearly in a two-hour range. It was expected that spermine concentrations would modulate protein biosynthesis selectively for the TTS-comprising TU. This modulation is attributed to spermine-stabilized triplex formation at the TTS, directly affecting mCerulean mRNA levels.

Figure 14 illustrates the transcription unit (TU) design and the role of spermine and TFOs in transcriptional regulation. Two identical TTSs are located between -35 to -10 and -10 to +1 relative to the transcription initiation site. These are the regions targeted by purine (Pu) or pyrimidine (Py) TFOs to form triplexes. Downstream of the transcription initiation site, the TU encodes mCerulean fluorescent protein, with a stop codon at the end of the open reading frame.

Fluorescence intensities directly correlate with mCerulean protein biosynthesis, indicating the effect of triplex formation and spermine concentrations on transcription and translation efficiency.

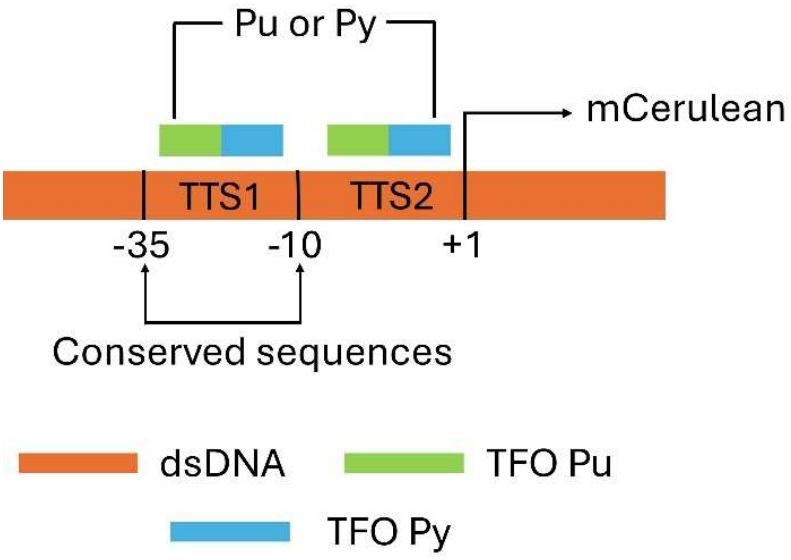


*Figure 14: Schematic representation of Transcription units with TTS1 and TTS2 regions targeted by TFOs. mCerulean fluorescence reflects transcriptional and translational efficiency.*

# 4. RESULTS

This chapter includes experimental results whose methods were described in chapter 3. EMSA, temperature-dependent denaturation analysis, molecular modelling, mass analysis, and *in vitro* transcription-translation results are presented.

## 4.1. Triplex Denaturation Analysis

Triplex denaturation experiments were performed following the protocol described in section 3.2.3. Figures 14, 15, 16, and 17 report temperature-dependent experimental fluorescence change rates (left panels) and normalized fluorescence peak intensity ratios (right panels) for TFO1-TTS and TFO2-TTS triplexes in the presence of spermine, spermidine, putrescine, or cadaverine, respectively. In the presence of spermine or spermidine, temperature-denaturation showed two distinct peaks corresponding to the thermal dissociation of the triplex and duplex structures, as illustrated schematically in Figure 13, section 3.2.3. On the other hand, Triplex Tm analysis in the presence of putrescine or cadaverine, Figures 16 and 17, respectively, did not show the typical two-peak profile, indicating no triplex formation. For this reason, these polyamines were not investigated further.

In a typical two-peak profile, triplex structures exhibited a lower melting temperature compared to duplexes, reflecting its reduced thermodynamic stability. Each peak in the denaturation profiles has a corresponding intensity that was used for the normalized intensity peak ratio analysis. It should be mentioned that experimental Tm values were found to be similar to Tm values calculated using the software Oligoanalyzer (Integrated DNA Technologies). Nevertheless, different polyamine concentrations affected the experimental Tm slightly, as can be seen in the experimental data. For this reason, the Tm value used for the normalized peak intensity ratio calculation was arbitrarily selected, taking into account the calculated and experimental values.

Tm values obtained from these analyses are collectively reported in Table 3. Normalized peak intensity ratio analysis produced EC50 values collectively reported in Table 4.

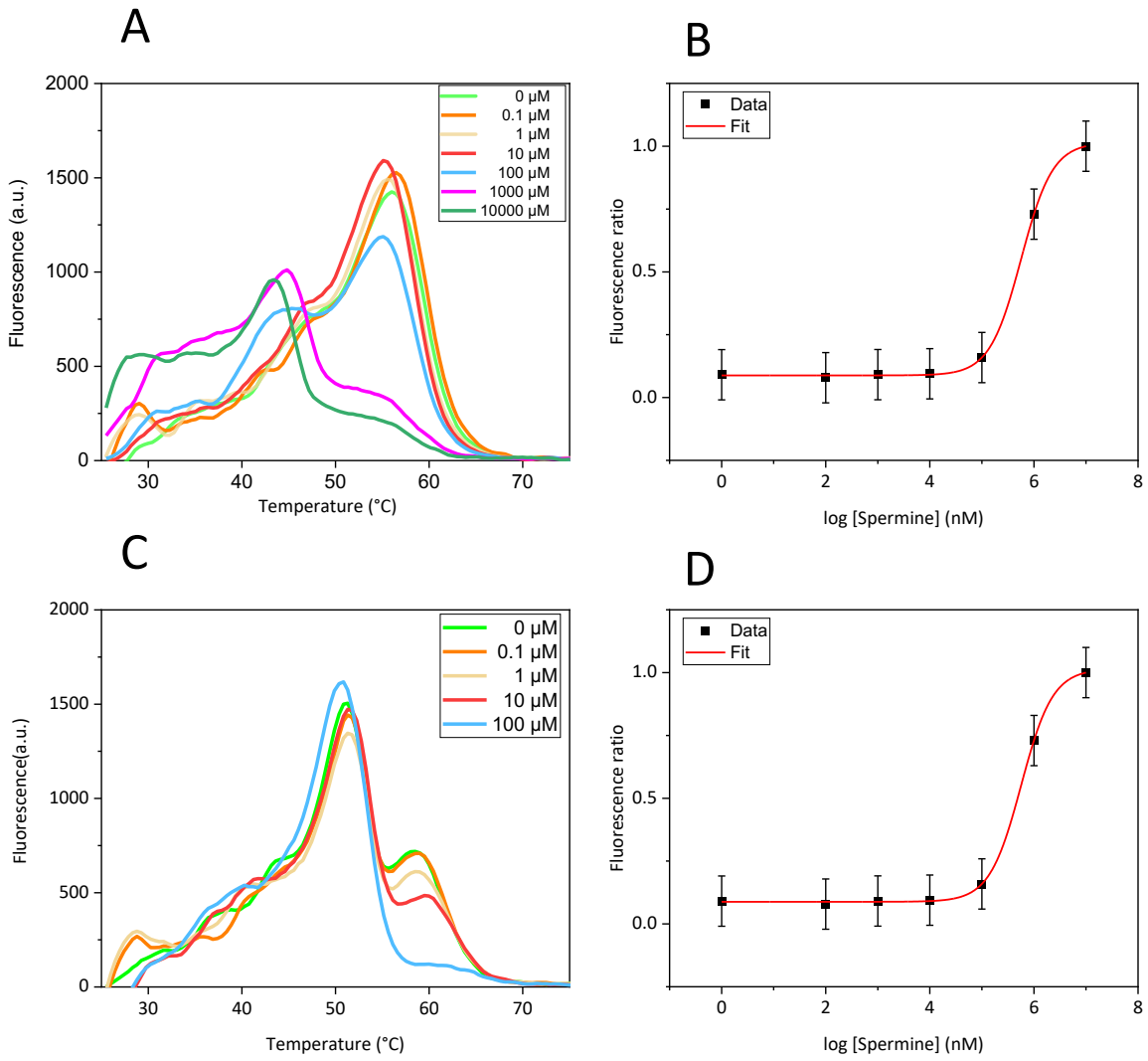


Figure 15: Experimental data of triplex and duplex denaturation. (A) Melting profiles of triplex and duplex structures for TFO1 (pyrimidine-rich) with increasing temperatures under varying Spm concentrations. (B) Peak intensity ratios plotted against Spm concentrations for TFO1. (C) Melting profiles of triplex and duplex structures for TFO2 (purine-rich) with increasing temperatures under varying Spm concentrations. (D) Peak intensity ratios plotted against Spm. concentrations for TFO2. Different colors represent distinct Spm concentrations.

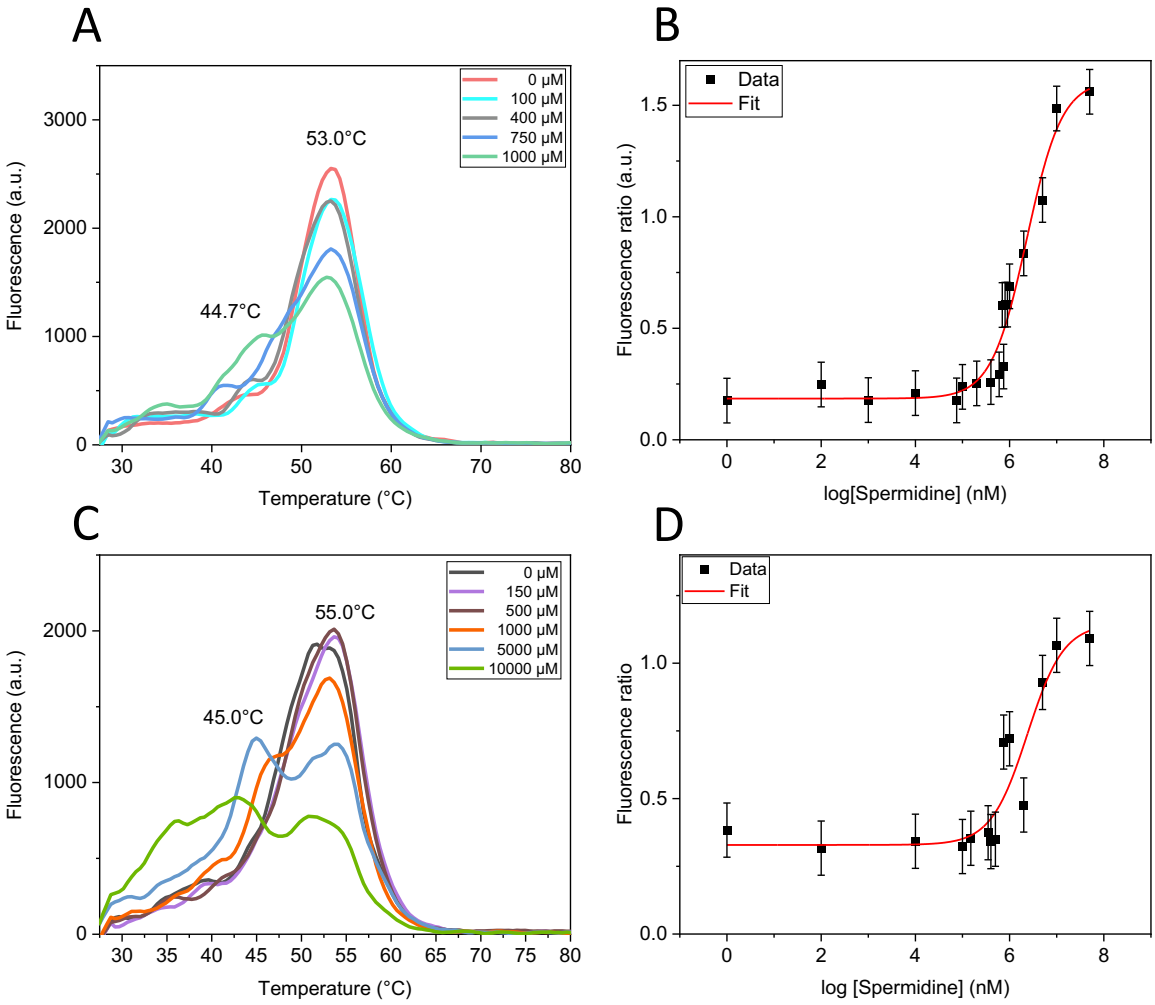


Figure 16: Experimental data of triplex and duplex denaturation. (A) Melting profiles of triplex and duplex structures for TFO1 (pyrimidine-rich) with increasing temperatures under varying Spd concentrations. (B) Peak intensity ratios plotted against Spd concentrations for TFO1. (C) Melting profiles of triplex and duplex structures for TFO2 (purine-rich) with increasing temperatures under varying Spd concentrations. (D) Peak intensity ratios plotted against Spd concentrations for TFO2. Different colors represent distinct Spd concentrations.

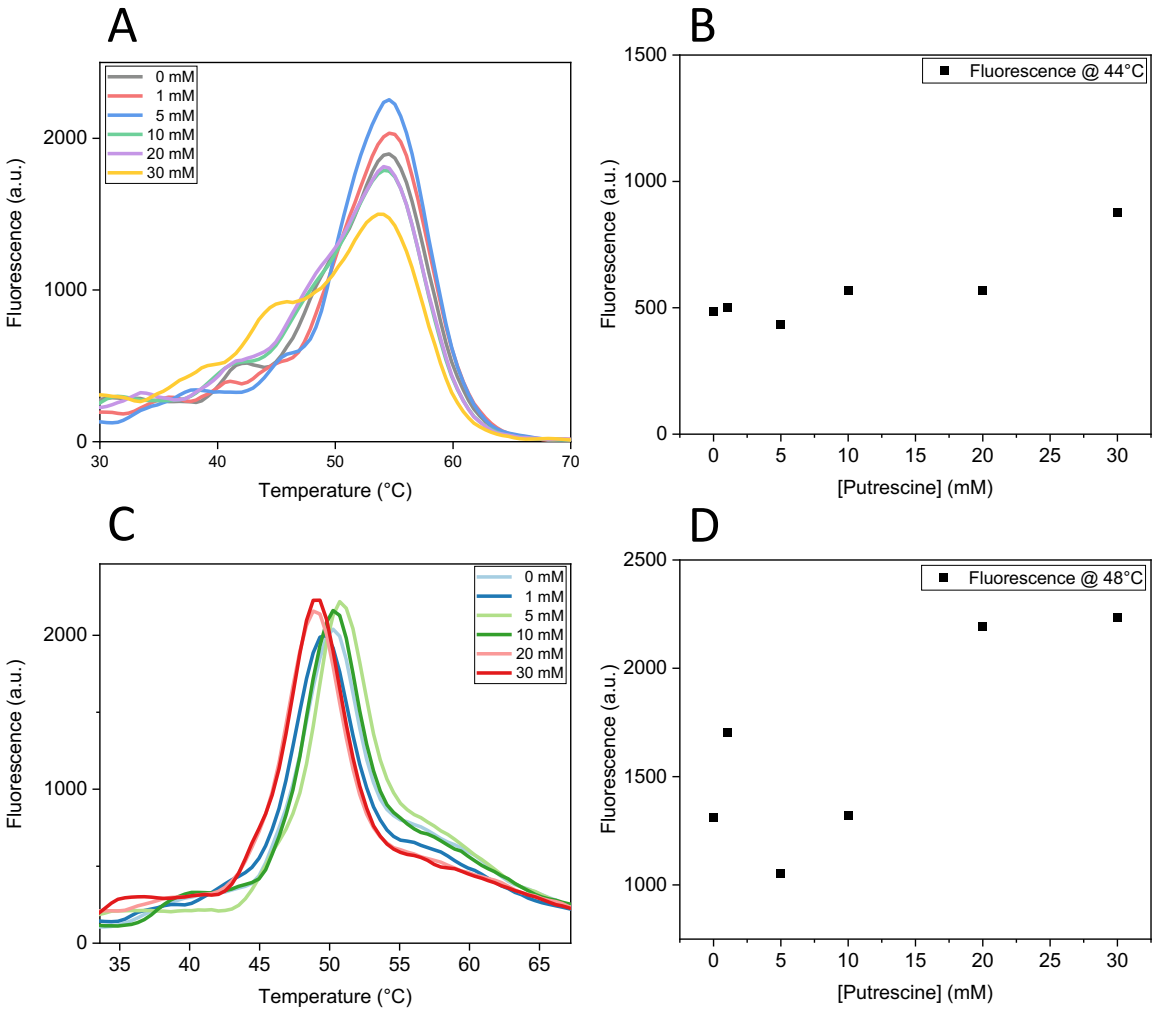


Figure 17: Experimental data of triplex and duplex denaturation. (A) Melting profiles of triplex and duplex structures for TFO1 (pyrimidine-rich) with increasing temperatures under varying Put concentrations. (B) Peak intensity ratios plotted against Put concentrations for TFO1. (C) Melting profiles of triplex and duplex structures for TFO2 (purine-rich) with increasing temperatures under varying Put concentrations. (D) Peak intensity ratios plotted against Put concentrations for TFO2. Different colors represent distinct Put concentrations.

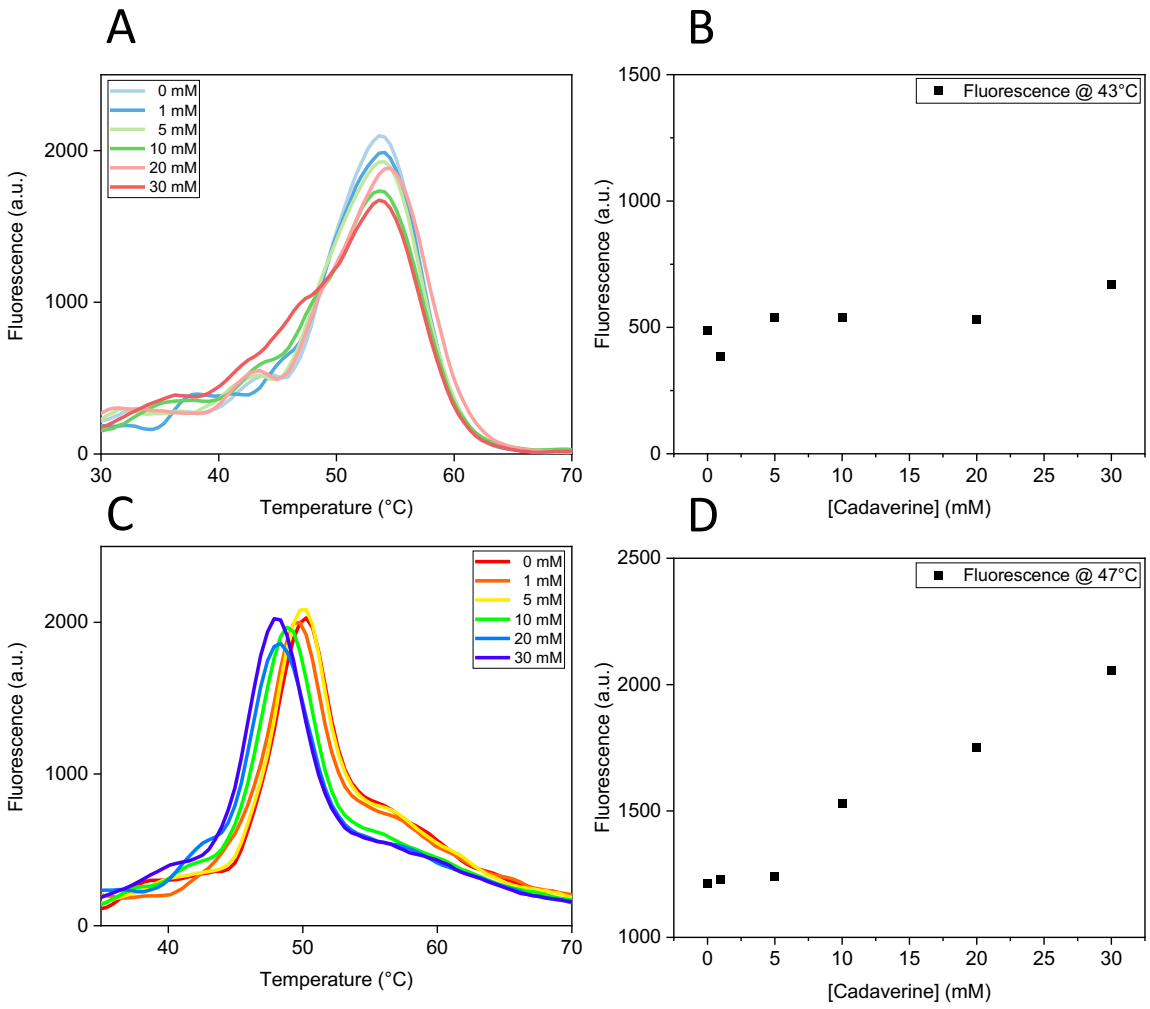


Figure 18: Experimental data of triplex and duplex denaturation. (A) Melting profiles of triplex and duplex structures for TFO1 (pyrimidine-rich) with increasing temperatures under varying Cdv concentrations. (B) Peak intensity ratios plotted against Cdv concentrations for TFO1. (C) Melting profiles of triplex and duplex structures for TFO2 (purine-rich) with increasing temperatures under varying Cdv concentrations. (D) Peak intensity ratios plotted against Cdv concentrations for TFO2. Different colors represent distinct Cdv concentrations.

*Table 4: Melting Temperatures (Tm) of TFOs and TTSs in the Presence of Polyamines (nd, not determined).*

| Polyamine | TFO Name | TFO Tm (°C) | TTS Tm (°C) |
|---|---|---|---|
| Spermine | TFO1 | 44.7 | 56 |
| | TFO2 | 53 | 63 |
| Spermidine | TFO1 | 44.7 | 53 |
| | TFO2 | 45 | 55 |
| Cadaverine | TFO1 | nd | 55 |
| | TFO2 | nd | 50 |
| Putrescine | TFO1 | nd | 55 |
| | TFO2 | nd | 50 |

*Table 5: $EC_{50}$ Values (nd, not determined).*

| Polyamine | TFO Name | $EC_{50}$ (mM) |
|---|---|---|
| Spermine | TFO1 | 3.5+/-0.1 |
| | TFO2 | 0.3+/-0.1 |
| Spermidine | TFO1 | 25.1+/-0.1 |
| | TFO2 | 5.9+/-0.1 |
| Cadaverine | TFO1 | nd |
| | TFO2 | nd |
| Putrescine | TFO1 | nd |
| | TFO2 | nd |

## **4.2.** Analysis of Triplex Formation Using EMSA

Electrophoresis experiments were conducted to evaluate the formation of DNA:DNA:RNA triplexes in the presence of spermine. Figures 14 illustrate the results for triplex formation using TFO1 (pyrimidine-rich) and TFO2 (purine-rich) sequences. To investigate the influence of spermine (Spm) on triplex stability, separate gels were conducted for each TFO under three conditions: without spermine (0 μM Spm), with 50 μM Spm, and with 100 μM Spm. The distinct bands observed in the gels correspond to the dsDNA target sequence (TTS), the triplex structure, and excess unbound TFO, as indicated by black, green, and red arrows, respectively.

As expected, the dsDNA band exhibited the highest electrophoretic mobility due to its smaller molecular size. A progressive decrease in intensity was observed for this band with increasing TFO concentrations, suggesting effective triplex formation. Conversely, the triplex band displayed a slower migration pattern and became more prominent with increasing TFO concentrations, indicative of its larger molecular weight and structural complexity. A third, slower-migrating band was observed, corresponding to excess, unbound TFO accumulating as a result of incomplete hybridization.

Quantitative analysis was performed by plotting band intensities against TFO concentrations and fitting the data to a sigmoidal curve. The dissociation constant ($K_d$) values were derived from the symmetry point of the sigmoidal curves and they are summarized in Tables 5 and 6. These values reveal that the effect of spermine varies depending on the TFO sequence. Specifically, for TFO2, the presence of 50 μM spermine led to a decrease in $K_d$, indicating enhanced triplex stability, while 100 μM spermine resulted in a slight destabilization. In contrast, TFO1 exhibited an increase in $K_d$ at 50 μM Spm, implying reduced triplex formation efficiency, whereas 100 μM Spm significantly enhanced stability by lowering the $K_d$ value.

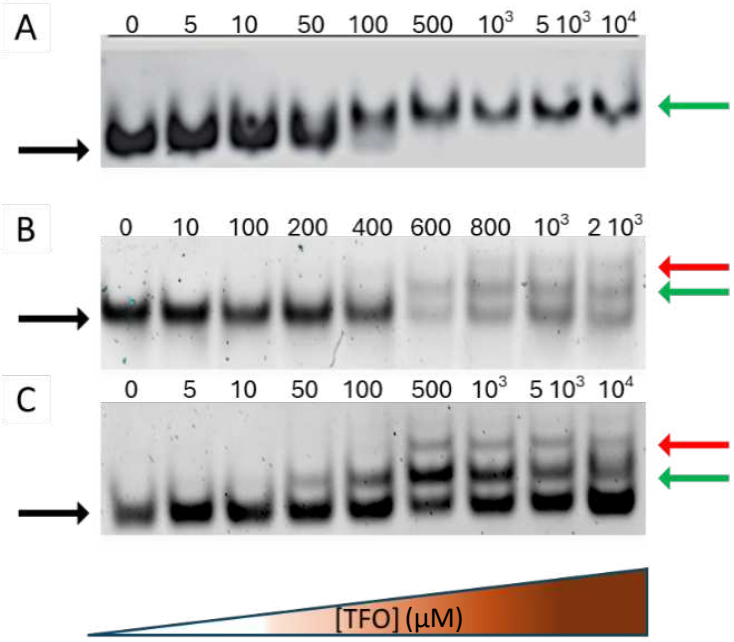


*Figure 19: Experimental data of EMSA analysis for TFO1 (pyrimidine-rich). Gel image of TTS incubated with varying TFO1 concentrations. (A) 0 µM Spm, (B) 50 µM Spm, and (C) 100 µM Spm. The black, green, and red arrows indicate the TTS, triplex, and unbound TFO bands, respectively.*

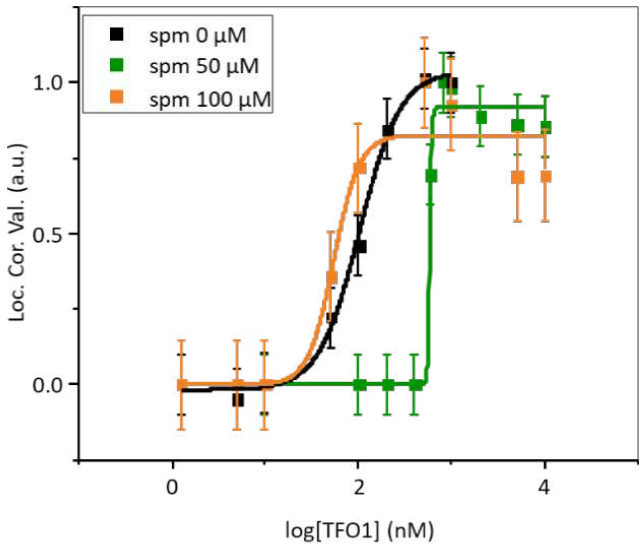


*Figure 20: Binding curve analysis of triplex formation. Band intensities from EMSA analysis were plotted against TFO1 concentrations and fitted to a sigmoidal curve for different Spm conditions: 0 µM Spm, 50 µM Spm, and 100 µM Spm.*

*Table 6: Kd values related to TFO1 in gel analysis*

| **[TTS ](nM)** | **[Spermine] (µM)** | **$K_d$ (nM)** |
|---|---|---|
| 100 | 0 | 100 ± 1 nM |
| | 50 | 582 nM ± 6 nM |
| | 100 | 54.6 nM ± 0.5 |

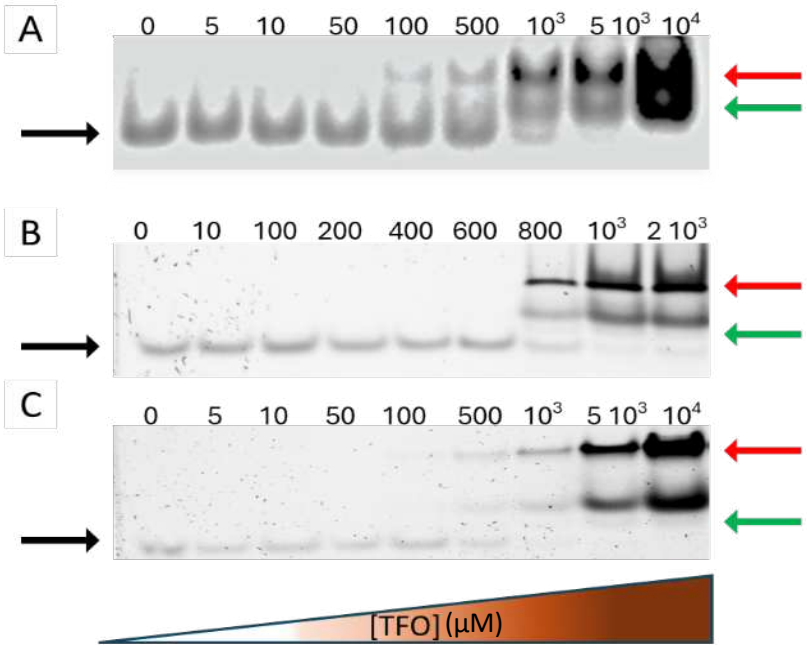


*Figure 21: Experimental data of EMSA analysis for TFO2 (purine-rich). Gel image of TTS incubated with varying TFO2 concentrations. (A) 0 μM Spm, (B) 50 μM Spm, and (C) 100 μM Spm. The black, green, and red arrows indicate the TTS, triplex, and unbound TFO bands, respectively.*

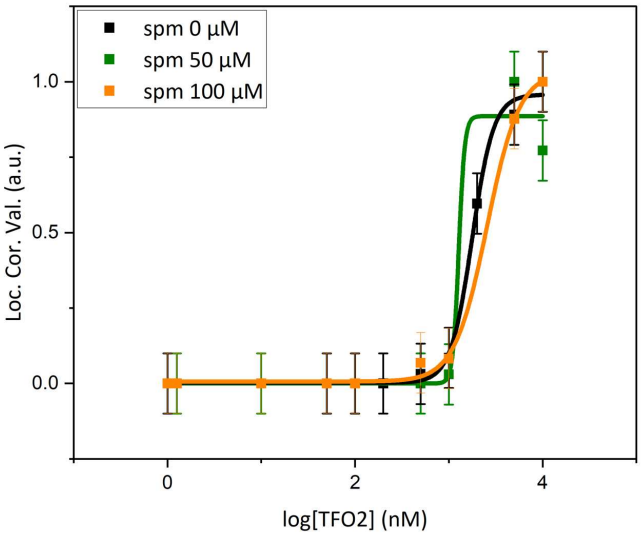


*Figure 22: Binding curve analysis of triplex formation. Band intensities from EMSA analysis were plotted against TFO2 concentrations and fitted to a sigmoidal curve for different Spm conditions: 0 μM Spm, 50 μM Spm, and 100 μM Spm.*

*Table 7: $K_d$ values related to TFO2 in gel analysis*

| **[TTS ](nM)** | **[Spermine] (μM)** | **$K_d$ (nM)** |
|---|---|---|
| 100 | 0 | 1.8 ± 0.2 uM |
| | 50 | 1.3 ± 0.1 uM |
| | 100 | 2.5 ± 0.3 uM |

## 4.3. Mass Spectrometry Analysis

To confirm formation of the RNA-DNA hybrid triplex complex, mass analysis was performed using the system described in the materials and methods section. Nucleic acids were incubated for one hour at 4°C to allow formation of the triplex structure in excess of Spm. Prior to analysis the sample was diluted 1:100 and immediately injected in the mass spectrometer. Figure 23 reports m/z peaks and peak deconvolution of triplex-control complex and Spm-incubated triplex. Along with the TFO peak at m/z= 1130, a weak signal supports the formation of an $8^-$-charged triplex complex (m/z= 1710, Panel A) and a signal deconvolution identifying a mass of ca. 13700Da (Panel B) which is expected for the triplex complex. On the other hand, when the triplex is incubated with Spm, more intense m/z peaks and peak deconvolution displayed in Panels C and D, identify a series of triplex+Spm complexes with triplex+1Spm, triplex+2Spm, and triplex+3Spm being the most representative.

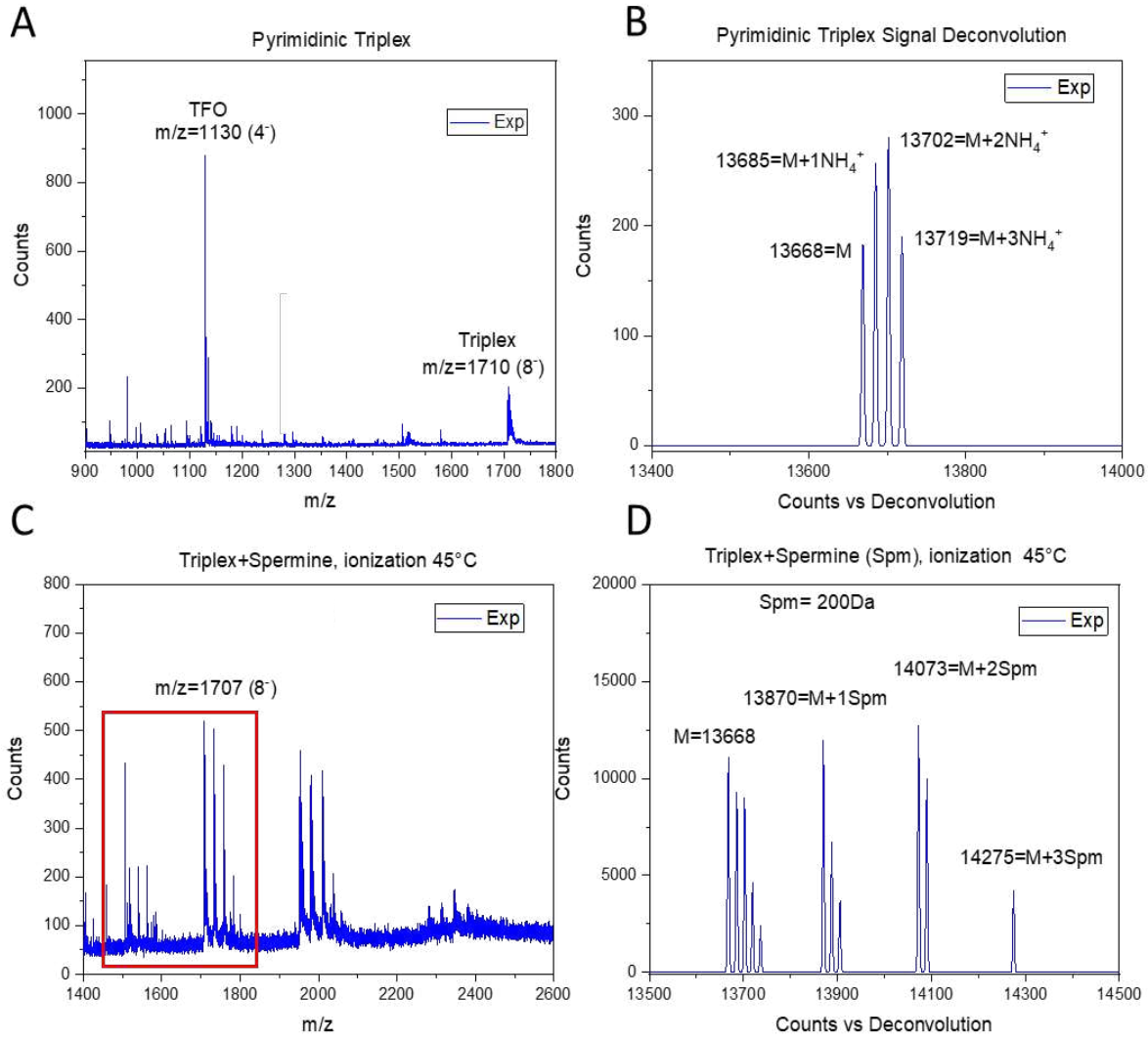


*Figure 23: Mass analysis results of pyrimidine triplex incubated with Spm. Panels A and B: m/z and peak deconvolution of triplex control without Spm. Panels C and D: m/z and peak deconvolution od Spm-incubated triplex.*

## 4.4. Molecular Modelling

Explorative molecular dynamics (MD) simulations were carried out on the representative purine RNA-DNA-DNA triplex. The system was prepared in a cubic box of 60 Å of side length, with the triplex in the middle, surrounded by 20 molecules of Spm placed and oriented randomly in space. As an example, the initial configuration for the system is reported in Figure 24.

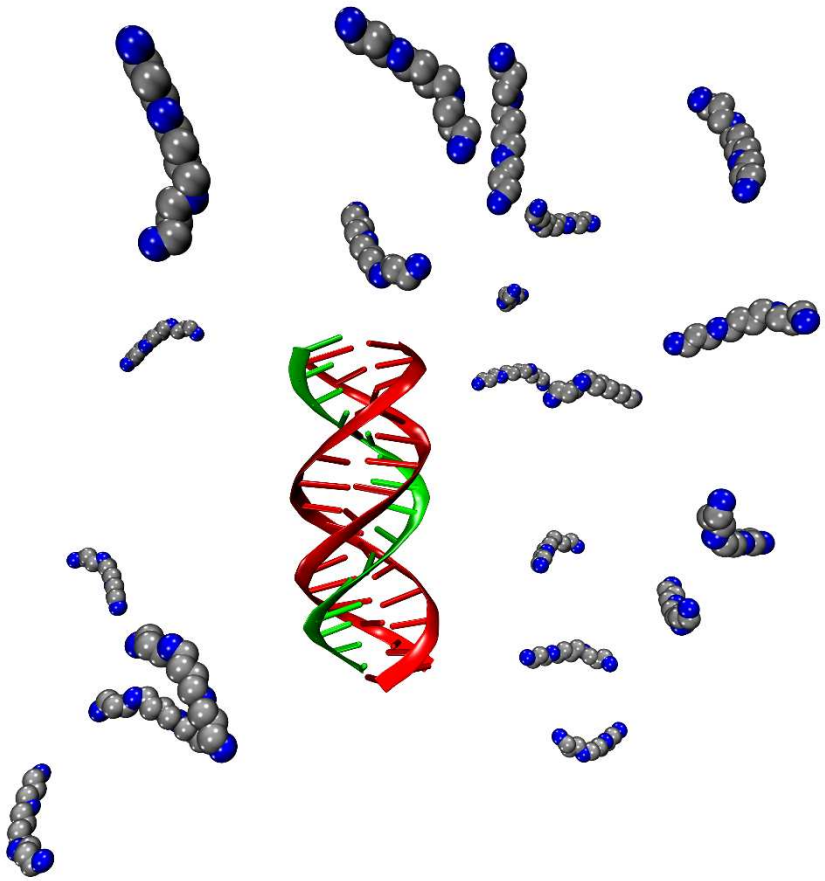

Figure 24: Initial configuration of the triplex system with 20 spermine molecules. DNA is represented as cartoon in red, RNA as cartoon in green, spermine molecules as spheres with radius set to the van der Waals radius of the atoms (heavy atoms only), C atoms in *gray, N atoms in blue.*

The MD simulations served to explore the geometries of binding of the spermine molecules to the triplex. Apart from the expected interaction with the major groove, spermine molecules can adopt different geometries especially in the terminal parts of the triplex. Figure 25 shows a representative Spm-triplex complex with Spm molecules color-coded with red indicating strong interactions while grey color indicates weak interactions with the triplex.

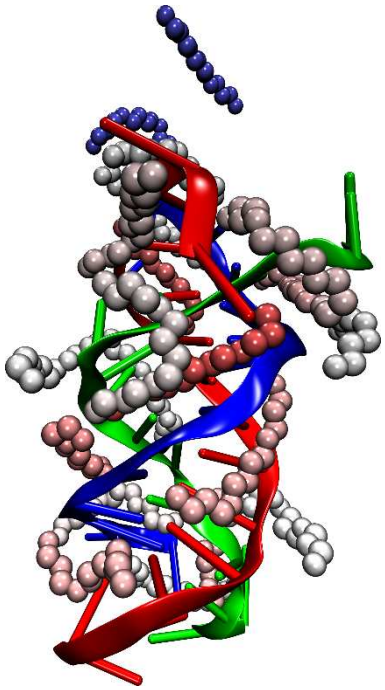

*Figure 25: Color mapping of the spermine molecules (represented as spheres) bound to the triplex comples. The triplex nucleic complex is represented as cartoon. Molecules with larger contact area (depicted in red) are those in the major groove.*

## 4.5. *In Vitro* Transcription-translation

Transcription units listed in Table 3 were used to produce mCerulean fluorescent protein *in vitro* to monitor rates of protein biosynthesis in a fluorescence plate reader. The amount of mRNA was assumed to be the rate limiting quantity and therefore by measuring protein synthesis rates, the relative abundance of mRNA could be estimated. Figures 26 and 27 show preliminary results of the protein biosynthetic rates for mCerulean from transcription units TU1 containing TTS regions and TU2 without TTS, in the presence of spermine (Spm) concentrations: 0, 100, or 200 µM. The effect of purine (Pu) or pyrimidine (Py) TFOs was evaluated by comparing relative biosynthetic rates of the two TUs in the same conditions. At 0 and 100 µM Spm, no statistically significant difference was observed between the two TUs. On the other hand, at 200 mM Spm concentration, TU1 showed enhanced production of mCerulean while no statistically significant difference was observed for TU2, compared to the control sample (CTR) containing no TFO.

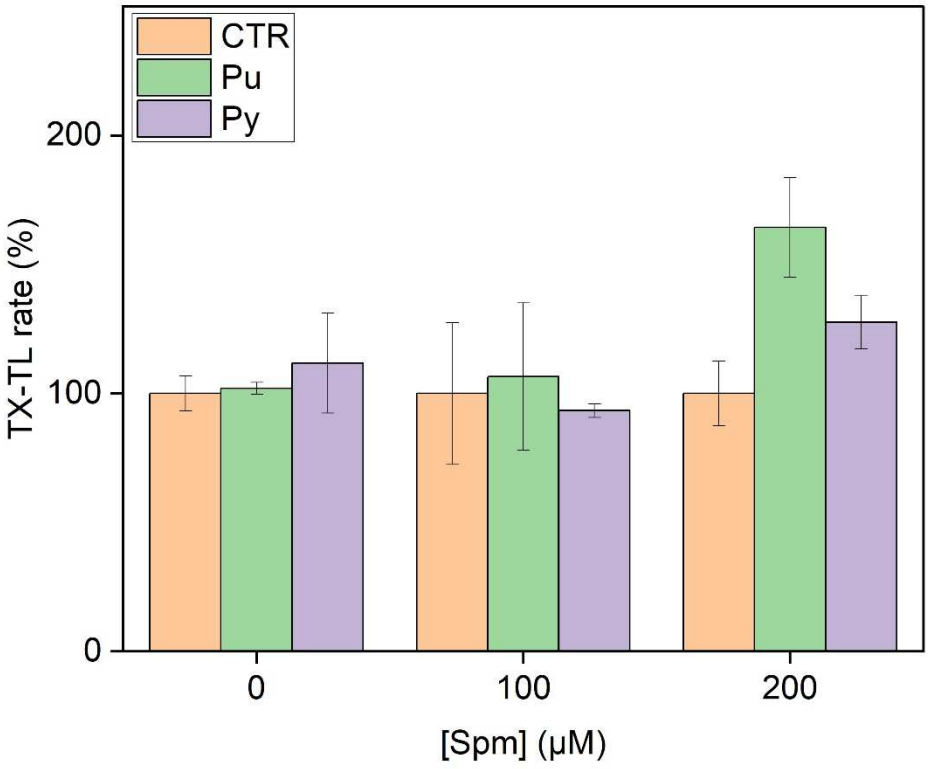


*Figure 26: In vitro transcription-translation of mCeruelan from the TTS-comprising TU1. Bars represent protein biosynthetic rates estimated from fluorescence changes at mCerulean emission, normalized to the control sample rate (CTR), without TFO. Average values of three independent experiments.*

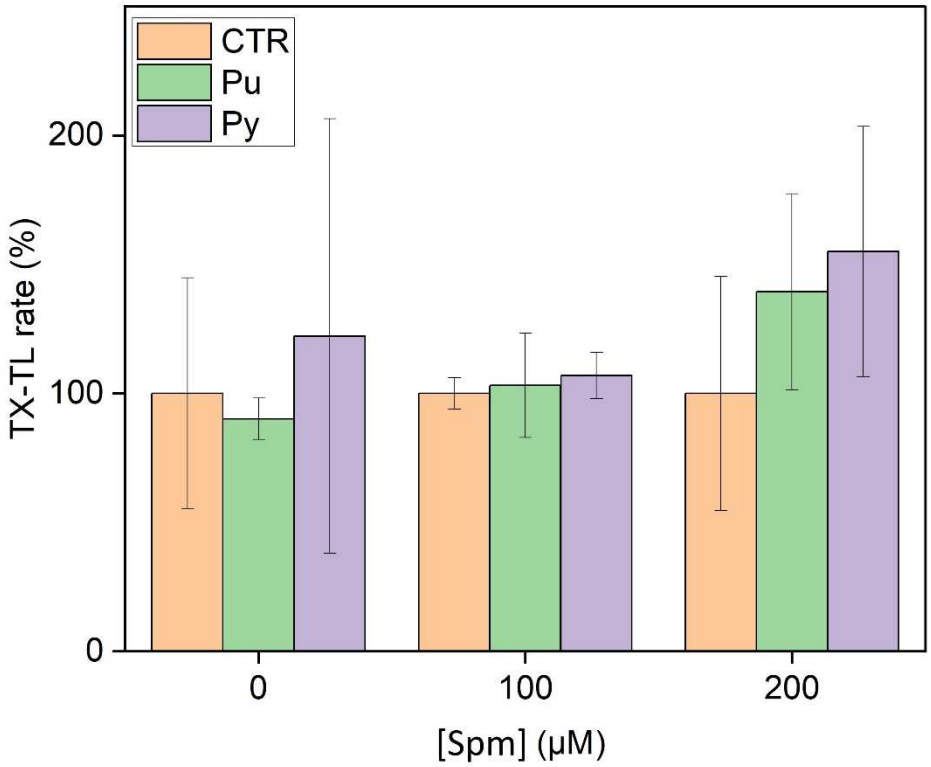


*Figure 27: In vitro transcription-translation of mCeruelan from the control TU2 without TTS. Bars represent protein biosynthetic rates estimated from fluorescence changes at mCerulean emission, normalized to the control sample rate, without TFO. Average values of three independent experiments.*

# 5. DISCUSSION

In this section, the results of EMSA, Tm analysis, mass analysis, and molecular modelling presented in the previous section will be discussed. In particular,

As reported in the results section, 15-nucleotide long designed RNA-DNA triplexes comprising a duplex DNA (TTS) and a single-strand RNA (TFO) were characterized by melting temperature (Tm) analysis and EMSA to estimate their thermodynamic stability. Specifically, since previous studies showed that metal ion-based (30 mM $Mg^{2+}$) high ionic strength stabilized the nucleic acid complex formation,[62] the goal was to demonstrate that polyamines could replace $Mg^{2+}$ in solution. Four polyamines were initially tested in Tm measurements: Spermine (Spm), spermidine, cadaverine, and putrescine. These polyamines are found inside cells, and among polyamines they are the most representative. Results of Tm analysis were used to extract normalized peak intensity ratios of the duplex and triplex denaturation peaks, as described in the methods section (see equation 3). Ratios were then plotted against polyamine concentration in a single-log plot and fitted with Eq. 2 sigmoid (Figures 15, 16, 17, and 18). The symmetry points of the sigmoid functions were then used to interpolate the corresponding polyamine concentration that was interpreted as $EC_{50}$ (effective concentration 50%), that is the concentration at which half-maximal effect is observed. Results collectively reported in Table 5 indeed show that Spm and Spd stabilize triplex formation with $EC_{50}$ values in the millimolar/sub-millimolar range, between 0.3 and 25 mM, depending on the type of triplex (i.e., pyrimidine or purine), with purine triplexes generally showing a ca. ten-fold lower $EC_{50}$ value. This is in line with polyamine content in cells, which is commonly in the millimolar range.[67], [68]
On the other hand, putrescine and cadaverine did not show any detectable effect, with temperature-dependent denaturation profiles only showing one peak, associated with duplex DNA dissociation and therefore pointing at a negligible triplex content, Figures 17 and 18. For this reason, and being Spm the polyamine associated with the stronger stabilization effects, the following experiments, i.e., EMSA and mass analysis, were conducted with the use of Spm only.
EMSA analysis was conducted using three conditions: 0, 50, and 100 μM spermine concentration. Samples containing a constant duplex DNA concentration and a range of TFO concentrations (see the methods section for the specific quantities) were separated in

native polyacrylamide gels, and bands corresponding to the triplex structure were quantified (Figures 19 and 21). Values corresponding to the triplex band intensities were then plotted against Spm concentration in a single-log plot. The experimental data points were then fitted with sigmoid Eq. 2 and the symmetry point of the function was used to interpolate the corresponding TFO concentration. Figures 20 and 22 report the sigmoidal fitting of the experimental points obtained from the separations in the three experimental conditions. These curves were used to estimate the $K_d$ value for triplex formation (i.e., TFO concentration at the symmetry point of the function). Results are collectively reported in Tables 6 and 7, showing (i) $K_d$ values of ca. 100 μM for pyrimidine TFO1 and ca. 2 mM for purine TFO2; (ii) a high variability of $K_d$ values for pyrimidine TFO1 and low variability for purine TFO2. EMSA results are substantially less conclusive than Tm analysis results, and for this reason they were considered only qualitatively. Indeed, they support triplex complex formation, but they cannot be used to evaluate $EC_{50}$ values as for Tm analysis.

Following this initial characterization, and to confirm triplex formation with an additional technique, mass analysis was performed. Results shown in Figure 23 demonstrate the formation of 1-, 2-, and 3-Spm comprising triplex complexes. It should be noted that although the triplex mass was detected also in the absence of spermine, the signal associated with the Spm-triplex complex was much higher than the triplex alone-associated signal. This supports the stabilizing effect of Spm towards the RNA-DNA triplex.

This, in addition to Tm and EMSA experimental results, provides a consistent set of data supporting the use of spermine as a replacement for metal ions as RNA-DNA triplex stabilizers.

To further strengthen this hypothesis, a molecular model of the RNA-DNA hybrid triplex was produced and integrated into a system of the possible Spm-triplex binding. Qualitative results are displayed as three-dimensional representations in Figure 25, showing a color-coded series of Spm molecules close to a triplex structure. Colors indicate a strong interaction (red) or weak interaction (grey). Indeed, three Spm molecules are strongly interacting with the triplex complex, while all other polyamine molecules are only weakly interacting with the triplex complex (grey-colored molecules), in accordance with mass spectrometry analysis.

In the final step of this work, transcription units (TUs) comprising a TTS-modified σ70 bacterial promoter consensus, TU1, or a σ70 bacterial promoter consensus, TU2, were used

to perform *in vitro* mCerulean transcription-translation experiments in the presence of TFOs and polyamines. Average biosynthetic rates of TUs containing the TTS or unable to form the triplex are reported in Figures 26 and 27, respectively, as mCerulean fluorescent protein emission change rates. Although results are affected by a large standard deviation, they clearly show that the presence of the TFOs at Spm concentrations of at least 100 μM have a modulating effect on protein biosynthetic rates only for the TTS-comprising TU1. This modulation was attributed to mCerulean mRNA levels, directly affected by triplex formation at the TTS-comprising promoter.

# 6. CONCLUSION AND PERSPECTIVES

This study has provided novel insights into the stabilization mechanisms of hybrid DNA-RNA triplexes, particularly emphasizing the role of polyamines in modulating their biophysical properties. By employing electrophoretic mobility shift assays (EMSA) and melting temperature (Tm) analysis, it was demonstrated that spermine significantly enhances the stability of these triplex structures. This effect was found to be more pronounced compared to other polyamines, reinforcing the hypothesis that spermine can serve as a functional substitute for high $Mg^{2+}$ concentrations previously required for in vitro stabilization. These findings were further supported by mass spectrometry, which confirmed spermine association with triplex-forming sequences, and by molecular modeling, which elucidated the potential binding interactions responsible for the observed stabilization effects.

Beyond the fundamental biophysical characterization, these preliminary experiments suggest a functional role for these triplexes in gene expression regulation. The *in vitro* production of the reporter protein mCerulean appeared to be modulated by triplex formation at the promoter of σ70 synthetic bacterial transcription units, under spermine concentrations exceeding 100 µM. While these findings remain preliminary, they open intriguing possibilities regarding the interplay between triplex stability and transcriptional control in prokaryotic systems.

These results contribute to the broader understanding of nucleic acid secondary and tertiary structures and their functional implications in gene regulation. The ability of spermine to replace $Mg^{2+}$ in stabilizing triplexes suggests a possible in vivo relevance, as spermine is abundant in cellular environments, particularly in rapidly dividing cells and certain organelles such as mitochondria. Given the role of polyamines in chromatin organization and nucleic acid interactions, our findings may have implications beyond triplex stability, extending to areas such as transcriptional regulation, RNA-based therapeutics, and the design of synthetic gene circuits.

Looking ahead, several key directions emerge for future research. First, a more systematic investigation of the effects of varying spermine concentrations on triplex stability and transcriptional modulation should be conducted. Expanding these studies to other bacterial and eukaryotic promoters could reveal whether this phenomenon is generalizable across different regulatory contexts. Second, *in vivo* validation of our in vitro findings would

be crucial to establish physiological relevance. Using bacterial or eukaryotic models engineered to express synthetic triplex-forming sequences would allow us to assess whether spermine-mediated stabilization influences gene expression in a cellular context.

Another promising avenue involves extending molecular modeling approaches to explore the structural basis of spermine interactions with different triplex motifs. High-resolution techniques such as X-ray crystallography or cryo-electron microscopy could provide a more detailed picture of the molecular determinants governing these interactions. Additionally, investigating the competition between spermine and other cellular factors, including $Mg^{2+}$ and histones, could further elucidate the regulatory mechanisms at play in triplex formation.

Finally, given the potential applications of triplex structures in synthetic biology, the findings presented in this thesis may aid in the rational design of nucleic acid-based switches and regulatory elements for gene expression control. The ability to modulate transcription through targeted triplex formation in a spermine-dependent manner could be leveraged for developing novel biosensors, genetic circuits, or therapeutic strategies aimed at controlling gene activity in specific cellular environments.

In conclusion, this work highlighted the stabilizing role of spermine in DNA-RNA triplex formation and provided preliminary evidence for its impact on gene expression. These findings pave the way for further exploration into the biological significance of triplex structures and their potential applications in molecular biology, biotechnology, and synthetic biology.

# **7.** REFERENCES


[1] S. Lu, Y. Tang, S. Yin, and L. Sun, 'RNA structure: implications in viral infections and neurodegenerative diseases', *Advanced Biotechnology*, vol. 2, no. 1, Feb. 2024, doi: 10.1007/s44307-024-00010-2.

[2] J. Barciszewski Editor, 'RNA Structure and Function RNA Technologies 14'.

[3] H. Follmann, 'Deoxyribonucleotides: the unusual chemistry and biochemistry of DNA precursors', *Chem Soc Rev*, vol. 33, no. 4, p. 225, 2004, doi: 10.1039/a907361b.

[4] G. D. Bowman and M. G. Poirier, 'Post-translational modifications of histones that influence nucleosome dynamics', Mar. 25, 2015, *American Chemical Society*. doi: 10.1021/cr500350x.

[5] D. Rhodes and H. J. Lipps, 'Survey and summary G-quadruplexes and their regulatory roles in biology', Oct. 15, 2015, *Oxford University Press*. doi: 10.1093/nar/gkv862.

[6] E. Smirnov, P. Molínová, N. Chmúrčiaková, T. Vacík, and D. Cmarko, 'Non-canonical DNA structures in the human ribosomal DNA', Dec. 01, 2023, *Springer Science and Business Media Deutschland GmbH*. doi: 10.1007/s00418-023-02233-1.

[7] S. R. Holbrook, 'RNA structure: The long and the short of it', 2005, *Elsevier Ltd*. doi: 10.1016/j.sbi.2005.04.005.

[8] Q. Zhao, Z. Zhao, X. Fan, Z. Yuan, Q. Mao, and Y. Yao, 'Review of machine learning methods for RNA secondary structure prediction', *PLoS Comput Biol*, vol. 17, no. 8, p. e1009291, Aug. 2021, doi: 10.1371/journal.pcbi.1009291.

[9] R. X. F. Chen, C. M. Reidys, and M. S. Waterman, 'RNA Secondary Structures with Given Motif Specification: Combinatorics and Algorithms', *Bull Math Biol*, vol. 85, no. 3, Mar. 2023, doi: 10.1007/s11538-023-01128-5.

[10] M. P. Crossley, M. Bocek, and K. A. Cimprich, 'R-Loops as Cellular Regulators and Genomic Threats', Feb. 07, 2019, *Cell Press*. doi: 10.1016/j.molcel.2019.01.024.

[11] E. S. Khan and S. Danckwardt, 'Pathophysiological Role and Diagnostic Potential of R-Loops in Cancer and Beyond', *Genes (Basel)*, vol. 13, no. 12, p. 2181, Nov. 2022, doi: 10.3390/genes13122181.

[12] E. Smirnov, P. Molínová, N. Chmúrčiaková, T. Vacík, and D. Cmarko, 'Non-canonical DNA structures in the human ribosomal DNA', Dec. 01, 2023, *Springer Science and Business Media Deutschland GmbH*. doi: 10.1007/s00418-023-02233-1.

[13] A. Rich and D. R. Davies, 'A NEW TWO STRANDED HELICAL STRUCTURE: POLYADENYLIC ACID AND POLYURIDYLIC ACID', *J Am Chem Soc*, vol. 78, no. 14, pp. 3548–3549, Jul. 1956, doi: 10.1021/ja01595a086.

[14] G. Felsenfeld, D. R. Davies, and A. Rich, 'FORMATION OF A THREE-STRANDED POLYNUCLEOTIDE MOLECULE', *J Am Chem Soc*, vol. 79, no. 8, pp. 2023–2024, Apr. 1957, doi: 10.1021/ja01565a074.

[15] M. Duca, P. Vekhoff, K. Oussedik, L. Halby, and P. B. Arimondo, 'The triple helix: 50 years later, the outcome', *Nucleic Acids Res*, vol. 36, no. 16, pp. 5123–5138, 2008, doi: 10.1093/nar/gkn493.

[16] M. D. Frank-Kamenetskii and S. M. Mirkin, 'TRIPLEX DNA STRUCTURES', *Annu Rev Biochem*, vol. 64, no. 1, pp. 65–95, Jun. 1995, doi: 10.1146/annurev.bi.64.070195.000433.

[17] R. Eritja, '5 Nucleic acids triple helices', in *Nucleic Acids Chemistry*, De Gruyter, 2021, pp. 187–230. doi: 10.1515/9783110639537-005.

[18] S. Khan, A. Singh, N. Nain, S. Gulati, and S. Kukreti, 'Sequence-specific recognition of a coding segment of humanDACH1geneviashort pyrimidine/purine oligonucleotides', *RSC Adv*, vol. 11, no. 63, pp. 40011–40021, Dec. 2021, doi: 10.1039/d1ra06604h.

[19] S. Jalali, A. Singh, S. Maiti, and V. Scaria, 'Genome-wide computational analysis of potential long noncoding RNA mediated DNA: DNA: RNA triplexes in the human genome', *J Transl Med*, vol. 15, no. 1, Sep. 2017, doi: 10.1186/s12967-017-1282-9.

[20] T. Mondal *et al.*, 'MEG3 long noncoding RNA regulates the TGF-β pathway genes through formation of RNA–DNA triplex structures', *Nat Commun*, vol. 6, no. 1, p. 7743, Jul. 2015, doi: 10.1038/ncomms8743.
[21] N. Sentürk Cetin, C.-C. Kuo, T. Ribarska, R. Li, I. G. Costa, and I. Grummt, 'Isolation and genome-wide characterization of cellular DNA:RNA triplex structures', *Nucleic Acids Res*, vol. 47, no. 5, pp. 2306–2321, Mar. 2019, doi: 10.1093/nar/gky1305.
[22] S. Kim and B. K. Kaang, 'Epigenetic regulation and chromatin remodeling in learning and memory', Jan. 13, 2017, *Nature Publishing Group*. doi: 10.1038/emm.2016.140.
[23] M. A. J. Morgan and A. Shilatifard, 'Reevaluating the roles of histone-modifying enzymes and their associated chromatin modifications in transcriptional regulation', *Nat Genet*, vol. 52, no. 12, pp. 1271–1281, Dec. 2020, doi: 10.1038/s41588-020-00736-4.
[24] X. Li, G. Egervari, Y. Wang, S. L. Berger, and Z. Lu, 'Regulation of chromatin and gene expression by metabolic enzymes and metabolites', Sep. 01, 2018, *Nature Publishing Group*. doi: 10.1038/s41580-018-0029-7.
[25] M. G. Daskalaki, C. Tsatsanis, and S. C. Kampranis, 'Histone methylation and acetylation in macrophages as a mechanism for regulation of inflammatory responses', *J Cell Physiol*, vol. 233, no. 9, pp. 6495–6507, Sep. 2018, doi: 10.1002/jcp.26497.
[26] P. L. deHaseth, M. L. Zupancic, and M. T. Record, 'RNA Polymerase-Promoter Interactions: the Comings and Goings of RNA Polymerase', *J Bacteriol*, vol. 180, no. 12, pp. 3019–3025, Jun. 1998, doi: 10.1128/JB.180.12.3019-3025.1998.
[27] D. F. Browning and S. J. W. Busby, 'The regulation of bacterial transcription initiation', *Nat Rev Microbiol*, vol. 2, no. 1, pp. 57–65, Jan. 2004, doi: 10.1038/nrmicro787.
[28] A. Feklístov, B. D. Sharon, S. A. Darst, and C. A. Gross, 'Bacterial Sigma Factors: A Historical, Structural, and Genomic Perspective', *Annu Rev Microbiol*, vol. 68, no. 1, pp. 357–376, Sep. 2014, doi: 10.1146/annurev-micro-092412-155737.
[29] A. Feklistov and S. A. Darst, 'Structural Basis for Promoter −10 Element Recognition by the Bacterial RNA Polymerase σ Subunit', *Cell*, vol. 147, no. 6, pp. 1257–1269, Dec. 2011, doi: 10.1016/j.cell.2011.10.041.
[30] A. N. Kapanidis, E. Margeat, S. O. Ho, E. Kortkhonjia, S. Weiss, and R. H. Ebright, 'Initial Transcription by RNA Polymerase Proceeds Through a DNA-Scrunching Mechanism', *Science (1979)*, vol. 314, no. 5802, pp. 1144–1147, Nov. 2006, doi: 10.1126/science.1131399.
[31] J. M. Peters, A. D. Vangeloff, and R. Landick, 'Bacterial Transcription Terminators: The RNA 3′-End Chronicles', *J Mol Biol*, vol. 412, no. 5, pp. 793–813, Oct. 2011, doi: 10.1016/j.jmb.2011.03.036.
[32] B. Liu and T. A. Steitz, 'Structural insights into NusG regulating transcription elongation', *Nucleic Acids Res*, vol. 45, no. 2, pp. 968–974, Jan. 2017, doi: 10.1093/nar/gkw1159.
[33] E. Song, S. Han, H. Uhm, C. Kang, and S. Hohng, 'Single-mode termination of phage transcriptions, disclosing bacterial adaptation for facilitated reinitiations', *Nucleic Acids Res*, vol. 52, no. 15, pp. 9092–9102, Aug. 2024, doi: 10.1093/nar/gkae620.
[34] A. Khatri and R. Sen, 'Functionally important components of the transcription elongation complex involved in Rho-dependent termination', *FEMS Microbiol Lett*, vol. 372, Jan. 2025, doi: 10.1093/femsle/fnae111.
[35] M. W. Webster *et al.*, 'Structural basis of transcription-translation coupling and collision in bacteria', *Science (1979)*, vol. 369, no. 6509, pp. 1355–1359, Sep. 2020, doi: 10.1126/science.abb5036.
[36] M. Guttman and J. L. Rinn, 'Modular regulatory principles of large non-coding RNAs', *Nature*, vol. 482, no. 7385, pp. 339–346, Feb. 2012, doi: 10.1038/nature10887.
[37] L. Ma, V. B. Bajic, and Z. Zhang, 'On the classification of long non-coding RNAs', *RNA Biol*, vol. 10, no. 6, pp. 924–933, Jun. 2013, doi: 10.4161/rna.24604.
[38] G. Arun, S. D. Diermeier, and D. L. Spector, 'Therapeutic Targeting of Long Non-Coding RNAs in Cancer', *Trends Mol Med*, vol. 24, no. 3, pp. 257–277, Mar. 2018, doi: 10.1016/j.molmed.2018.01.001.

[39] Y. Fang and M. J. Fullwood, 'Roles, Functions, and Mechanisms of Long Non-Coding RNAs in Cancer', *Genomics Proteomics Bioinformatics*, vol. 14, no. 1, pp. 42–54, Feb. 2016, doi: 10.1016/j.gpb.2015.09.006.
[40] A. E. Pegg, 'Mammalian polyamine metabolism and function', *IUBMB Life*, vol. 61, no. 9, pp. 880–894, Sep. 2009, doi: 10.1002/iub.230.
[41] H. M. Wallace, 'Polyamines and their role in human disease – an introduction', *Biochem Soc Trans*, vol. 31, no. 2, pp. 354–355, Apr. 2003, doi: 10.1042/bst0310354.
[42] T. E. Dever and I. P. Ivanov, 'Roles of polyamines in translation', Nov. 30, 2018, *American Society for Biochemistry and Molecular Biology Inc.* doi: 10.1074/jbc.TM118.003338.
[43] K. Igarashi and K. Kashiwagi, 'Modulation of cellular function by polyamines', *Int J Biochem Cell Biol*, vol. 42, no. 1, pp. 39–51, Jan. 2010, doi: 10.1016/j.biocel.2009.07.009.
[44] T. J. Thomas, H. A. Tajmir-Riahi, and T. Thomas, 'Polyamine–DNA interactions and development of gene delivery vehicles', Oct. 01, 2016, *Springer-Verlag Wien*. doi: 10.1007/s00726-016-2246-8.
[45] S. Perepelytsya, J. Uličný, A. Laaksonen, and F. Mocci, 'Pattern preferences of DNA nucleotide motifs by polyamines putrescine2+, spermidine3+ and spermine4+', *Nucleic Acids Res*, vol. 47, no. 12, pp. 6084–6097, Feb. 2019, doi: 10.1093/NAR/GKZ434.
[46] F. Madeo, T. Eisenberg, F. Pietrocola, and G. Kroemer, 'Spermidine in health and disease', *Science (1979)*, vol. 359, no. 6374, Jan. 2018, doi: 10.1126/science.aan2788.
[47] A. E. Pegg, 'Functions of polyamines in mammals', Jul. 15, 2016, *American Society for Biochemistry and Molecular Biology Inc.* doi: 10.1074/jbc.R116.731661.
[48] N. Minois, D. Carmona-Gutierrez, and F. Madeo, 'Polyamines in aging and disease', *Aging*, vol. 3, no. 8, pp. 716–732, Aug. 2011, doi: 10.18632/aging.100361.
[49] T. Thomas* and T. J. Thomas, 'Polyamines in cell growth and cell death: molecular mechanisms and therapeutic applications', *Cellular and Molecular Life Sciences*, vol. 58, no. 2, pp. 244–258, Feb. 2001, doi: 10.1007/PL00000852.
[50] T. Nishio *et al.*, 'K+ promotes the favorable effect of polyamine on gene expression better than Na+', *PLoS One*, vol. 15, no. 9, p. e0238447, Sep. 2020, doi: 10.1371/journal.pone.0238447.
[51] M. D. Engstrom and B. F. Pfleger, 'Transcription control engineering and applications in synthetic biology', Sep. 01, 2017, *KeAi Communications Co.* doi: 10.1016/j.synbio.2017.09.003.
[52] J. Chappell, K. E. Watters, M. K. Takahashi, and J. B. Lucks, 'A renaissance in RNA synthetic biology: new mechanisms, applications and tools for the future', *Curr Opin Chem Biol*, vol. 28, pp. 47–56, Oct. 2015, doi: 10.1016/j.cbpa.2015.05.018.
[53] A. Cecconello, M. Magro, F. Vianello, and F. C. Simmel, 'Rational design of hybrid DNA–RNA triplex structures as modulators of transcriptional activity *in vitro*', *Nucleic Acids Res*, vol. 50, no. 22, pp. 13172–13182, Dec. 2022, doi: 10.1093/nar/gkac1131.
[54] D. Jeong *et al.*, 'Cell-Free Synthetic Biology Platform for Engineering Synthetic Biological Circuits and Systems.', *Methods Protoc*, vol. 2, no. 2, May 2019, doi: 10.3390/mps2020039.
[55] D. Jeong *et al.*, 'Cell-free synthetic biology platform for engineering synthetic biological circuits and systems', 2019, *MDPI AG*. doi: 10.3390/mps2020039.
[56] J. Kim, J. J. Hopfield, and E. Winfree, 'Neural Network Computation by In Vitro Transcriptional Circuits. Neural network computation by in vitro transcriptional circuits', 2004. [Online]. Available: https://www.researchgate.net/publication/220270163
[57] R. M. Murray, 'Subsystem Integration for Design and Implementation of Synthetic Cells'.
[58] R. K. Singh *et al.*, 'The junction of biomaterials and gene therapy - current strategies and future directions', in *Integration of Biomaterials for Gene Therapy*, wiley, 2023, pp. 323–348. doi: 10.1002/9781394175635.ch11.

[59] L. M. Hellman and M. G. Fried, 'Electrophoretic mobility shift assay (EMSA) for detecting protein–nucleic acid interactions', *Nat Protoc*, vol. 2, no. 8, pp. 1849–1861, Aug. 2007, doi: 10.1038/nprot.2007.249.
[60] J. R. Lakowicz, *Principles of fluorescence spectroscopy*. Springer, 2006. doi: 10.1007/978-0-387-46312-4.
[61] P.-C. Yang and T. Mahmood, 'Western blot: Technique, theory, and trouble shooting', *N Am J Med Sci*, vol. 4, no. 9, pp. 429–434, 2012, doi: 10.4103/1947-2714.100998.
[62] A. Cecconello, M. Magro, F. Vianello, and F. C. Simmel, 'Rational design of hybrid DNA–RNA triplex structures as modulators of transcriptional activity in vitro', *Nucleic Acids Res*, vol. 50, no. 22, pp. 13172–13182, Dec. 2022, doi: 10.1093/nar/gkac1131.
[63] H. S. Rye, B. L. Drees, H. C. M. Nelson, and A. N. Glazer, 'Stable fluorescent dye-DNA complexes in high sensitivity detection of protein-DNA interactions: Application to heat shock transcription factor', *Journal of Biological Chemistry*, vol. 268, no. 33, pp. 25229–25238, Nov. 1993, doi: 10.1016/s0021-9258(19)74592-x.
[64] J. C. Phillips *et al.*, 'Scalable molecular dynamics on CPU and GPU architectures with NAMD', *J Chem Phys*, vol. 153, no. 4, Jul. 2020, doi: 10.1063/5.0014475.
[65] S. Jo, T. Kim, V. G. Iyer, and W. Im, 'CHARMM-GUI: A web-based graphical user interface for CHARMM', *J Comput Chem*, vol. 29, no. 11, pp. 1859–1865, Aug. 2008, doi: 10.1002/jcc.20945.
[66] M. L. Markwardt *et al.*, 'An Improved Cerulean Fluorescent Protein with Enhanced Brightness and Reduced Reversible Photoswitching', *PLoS One*, vol. 6, no. 3, p. e17896, Mar. 2011, doi: 10.1371/journal.pone.0017896.
[67] A. J. Michael, 'Polyamines in eukaryotes, bacteria, and archaea', 2016. doi: 10.1074/jbc.R116.734780.
[68] K. Igarashi and K. Kashiwagi, 'Polyamines: Mysterious Modulators of Cellular Functions', *Biochem Biophys Res Commun*, vol. 271, no. 3, pp. 559–564, May 2000, doi: 10.1006/bbrc.2000.2601.
[69] Y. Mikame and A. Yamayoshi, 'Recent Advancements in Development and Therapeutic Applications of Genome-Targeting Triplex-Forming Oligonucleotides and Peptide Nucleic Acids', *Pharmaceutics*, vol. 15, no. 10, p. 2515, Oct. 2023, doi: 10.3390/pharmaceutics15102515.
[70] J. Kim and F. C. Simmel, 'Scaling up genelet circuits', *Nat Chem*, vol. 14, no. 11, pp. 1210–1211, Nov. 2022, doi: 10.1038/s41557-022-01069-x.